Plasma membrane transporter Progressive Ankylosis Protein Homolog (*ANKH*/*Ankh*) mediates senescence-derived extracellular citrate and is regulated by DNA damage, inflammation and ageing

Emma Naomi James[1], Muy-Teck Teh[1], Yufeng Li[2] Christine Wagner-Bock[3], Zahra Falah Al-Khateeb[4], Lee Peng Karen-Ng[1a], Terry Roberts[5], Linnea Synchyshyn[1], Amy Lewis[6], Ana O'Loghlen[7b], Andrew Silver[6], Adina Teodora Michael-Titus[4], Mark Bennett[8], Jacob Guy Bundy[2], Maria Elzbieta Mycielska[9c] and Eric Kenneth Parkinson[1,10]

[1]Centre for Oral Immunology and Regenerative Medicine, Institute of Dentistry, Barts and the London School of Medicine and Dentistry, Queen Mary University of London, Turner Street, London E1 2AD, UK

[2]Department of Metabolism, Digestion and Reproduction, Burlington Danes Building, Imperial College London, London W12 0NN, UK

[2]Universitätsklinikum Regensburg, Department of Dermatology, Forschungsbau H4 / R.41, Franz-Josef-Strauß Allee 11, 93053 Regensburg, Germany

[4]Centre for Neuroscience, Surgery and Trauma, Blizard Institute, 4 Newark Street, London E1 2AT

[4] Centre for Genome Engineering and Maintenance, Division of Biosciences, Department of Life Sciences, College of Health and Life Sciences, Brunel University London, Uxbridge, UB8 3PH, UK

[6]Centre for Genomics and Child Health, Colorectal Cancer Genetics Group, Blizard Building, 4 Newark Street, London E1 2AT

[7]Centre for Genomics and Child Health, Blizard Building, 4 Newark Street London E1 2AT

[8]Department of Life Sciences, South Kensington, Imperial College London, London SW7 2AZ,

[9]Department of Structural Biology, Institute of Biophysics and Physical Biochemistry, University of Regensburg, Universitätsstrasse 31, D-93053, Regensburg, Germany

[10]Correspondence to: Eric Kenneth Parkinson

Centre for Oral Immunology and Regenerative Medicine, Institute of Dentistry, Blizard Institute, 4 Newark Street, London E1 2AT UK, Phone: 44-(0)207-882-7185 Fax: 44(0)207-882-7137, Email: e.k.parkinson@qmul.ac.uk

[a] Present address:

Oral Cancer Research & Coordinating Centre (OCRCC), Faculty of Dentistry, Universiti Malaya, 50603 Kuala Lumpur, Malaysia.

[b] Present address: Centre for Biological Research (CIB)

Spanish National Research Council (CSIC)

Calle Ramiro de Maeztu 9, 28040 Madrid, SPAIN

Tel: +34 911 098 040

[c] Present address: MetaSMIte, Sp. z o.o. Krakow, Poland

Abstract

Citrate is produced by the tricarboxylic acid (TCA) cycle and, as a nutrient, can have both positive and negative effects on age-related disease. Citrate enters cells through plasma membrane transporters such as SLC13A5/I'm Not Dead Yet (INDY) and accumulates outside certain types of senescent cells *in vitro* and *in vivo* following telomere attrition. However, the detailed mechanism of senescent cell extracellular citrate (EC) accumulation is not clear. We show here that EC is mediated by a newly described plasma membrane citrate transporter *ANKH/SLC62A1* (progressive human ankylosis -*ANKH*) in senescent fibroblasts. Analogous to interleukin 6 (IL-6), EC and/or *ANKH* are regulated by telomere dysfunction, the p38 mitogen-activated kinase axis and transforming growth factor beta, but not by steroids or Ataxia Telangiectasia Mutated (ATM). However, the effect of sodium butyrate-induced senescence and p53 restraint on EC were variable and unrelated to *ANKH* expression. *ANKH* was also upregulated in senescent human astrocytes, adipocytes and myoblasts, but not pre-adipocytes or keratinocytes. Neither EC nor *ANKH* were regulated during keratinocyte differentiation. Surprisingly, EC and *ANKH* were inhibited in dividing and senescent fibroblasts by interleukin 1α (IL-1α) in parallel with increased IL-6 secretion. Interestingly, *Ankh* is downregulated in both aged mouse liver and brain tissues in parallel with increased senescence markers and the cytokines IL-1β, IL-6 and TNFα, suggesting that high levels of SASP cytokines could inhibit EC production *in vivo*. These data identify *ANKH*/*Ankh* as a novel regulator of senescence-derived EC in both humans and mice.

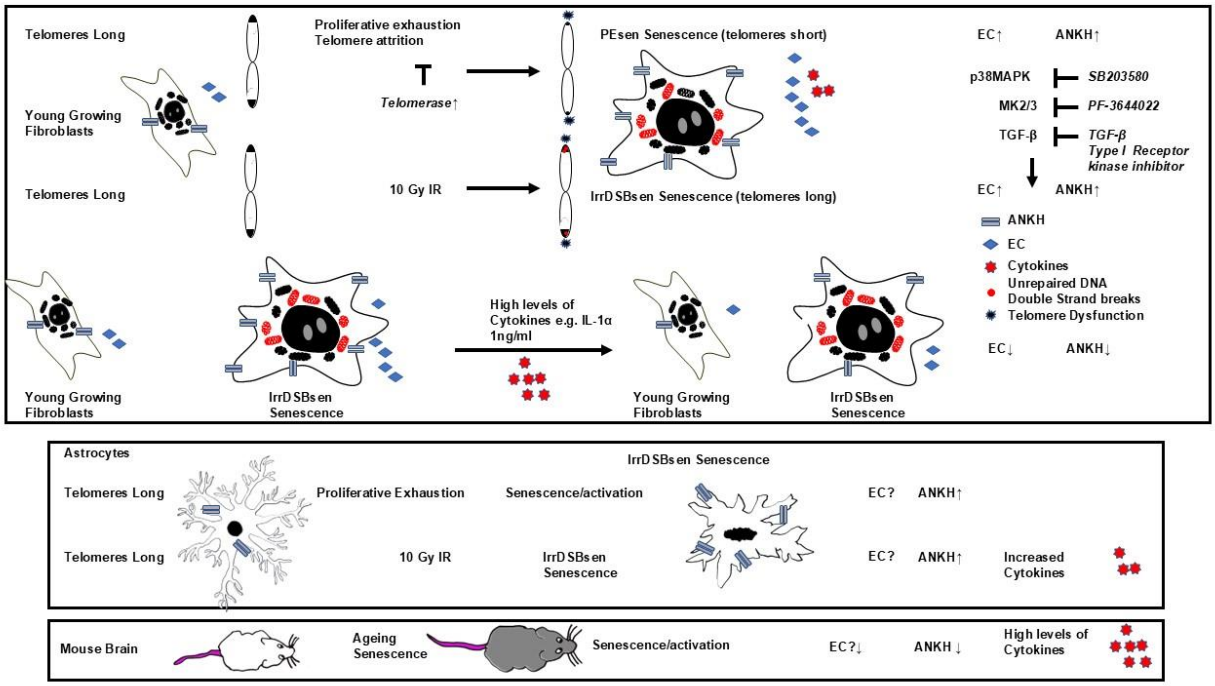
Telomeres Long
Young Growing Fibroblasts
Telomeres Long
Proliferative exhaustion
Telomere attrition
T
Telomerase↑
10 Gy IR
PEsen Senescence (telomeres short)
IrrDSBsen Senescence (telomeres long)
EC↑
ANKH↑
p38MAPK
SB203580
MK2/3
PF-3644022
TGF-β
TGF-β Type I Receptor kinase inhibitor
EC↑
ANKH↑
ANKH
EC
Cytokines
Unrepaired DNA Double Strand breaks
Telomere Dysfunction
EC↓
ANKH↓
Young Growing Fibroblasts
IrrDSBsen Senescence
High levels of Cytokines e.g. IL-1α 1ng/ml
Young Growing Fibroblasts
IrrDSBsen Senescence

Astrocytes
IrrDSBsen Senescence
Telomeres Long
Proliferative Exhaustion
Senescence/activation
EC?
ANKH↑
Telomeres Long
10 Gy IR
IrrDSBsen Senescence
EC?
ANKH↑
Increased Cytokines

Mouse Brain
Ageing Senescence
Senescence/activation
EC?↓
ANKH ↓
High levels of Cytokines

Introduction

Senescent cells are important to the progression of a wide variety of age-related conditions including Alzheimer's disease, Parkinson's disease, atherosclerosis, osteoporosis, osteoarthritis, frailty, type 2 diabetes, memory loss, hepatic steatosis and cancer(1). The deletion of senescent cells in mice slows but does not halt ageing and ameliorates but does not prevent age-related conditions. However, the understanding of the mechanisms by which senescent cells contribute to these diseases, especially in human subjects, remains incomplete.

Calorie intake regulates ageing in a variety of species including primates (2), and caloric restriction reduces the number of senescent cells and the inflammatory cytokines of the senescence associated secretory phenotype (SASP), in both mice and humans (3, 4). Therefore, the supply of energy metabolites may be partially responsible for both cellular senescence and ageing. One such metabolite is citrate, which accumulates over time in the body fluids of both humans (5) (reviewed in (6)) and mice (7, 8), including cerebrospinal fluid (5) and urine (7). A considerable body of recent evidence now supports citrate uptake as a major regulator of organismal lifespan and health span (9-14), including development of cancer(15, 16). Moreover, the upregulation of citrate uptake in mice by the ectopic expression of the mouse orthologue of *SLC13A5/INDY*, *SLC13A5/Mindy* induces a progeria-like phenotype and cellular senescence in the liver, via an increase in cytoplasmic citrate coupled with altered endoplasmic reticulum (ER) acetylation through SLC33A1(17). Notably, a similar ectopic expression of the mitochondrial membrane symporter *SLC25A1* did not elicit the same phenotypes despite producing similar levels of cytoplasmic citrate (17). Interestingly, alleviating ER stress is now thought to delay the formation of senescent cells *in vitro* and *in vivo* (18). However, whilst loss of function mutations in *SLC13A5/Mindy* protect mice against type 2 diabetes(9), high blood pressure (13), elevated heart rate (13) and memory loss (12), equivalent mutations in *SLC13A5/INDY* predispose humans to several developmental defects, including neonatal epilepsy, and the functions of the two transporters are somewhat different (19, 20). Furthermore, extracellular citrate (EC) can be

protective to mouse bone (21), kidneys (22) and the nervous system (11) in certain contexts. Therefore, it is currently unclear whether citrate is beneficial or detrimental to health and in which context.

Our previous work has shown that EC is upregulated following the proliferative exhaustion (PEsen) or irreparable DNA double strand break (IrrDSBsen)-induced senescence of several fibroblast lines from different tissue sites (23, 24) and is regulated by telomerase *in vitro* and in the human disease Dyskeratosis Congenita *in vivo* (25). A simple explanation for this increase in EC is that senescent fibroblasts (23) and melanocytes (26), but not breast epithelial cells (27), shift their energy metabolism towards glycolysis, as intracellular citrate inhibits phosphofructokinases 1 and 2 and hence glycolysis (28). Furthermore, inhibiting glycolysis may slow senescence *in vitro*(26, 29) and improve diabetic wound repair in mice (29). Consequently, citrate transport and glycolysis may represent ways of slowing the senescent cell production and ageing, but the mechanism of EC production by senescent cells and its importance for healthy aging remain unclear.

Recently, a plasma membrane transporter Progressive Ankylosis Protein Homolog *ANKH/SLC62A1* (*ANKH*) previously known to transport pyrophosphate was shown to export citrate and to a lesser extent malate and succinate (30). However, our previous work found that senescent fibroblasts do not show elevated levels of inorganic phosphate or pyrophosphate (23). *ANKH* loss-of-function mutations lead to ankylosis due to the retention of pyrophosphate in the bone (31), but *Ankh* knockout mice (30) and humans with loss of *ANKH* function (32) also have lower levels of plasma and urine citrate. In addition, a recent extensive genome-wide association screen revealed an association of the *ANKH* gene with a risk of developing Alzheimer's disease (33). Overall, ANKH appeared to be a good candidate for a role in citrate export in senescent cells.

We report that *ANKH* and EC are upregulated in a variety of senescent cells and that both were regulated in a similar manner to the SASP proteins. However, unlike SASP proteins, the

upregulation of EC and *ANKH* was cell type- and mechanism-specific. Our results identify an important role for *ANKH*/*Ankh* in the regulation of EC in many types of senescent cell and by inference, age-related diseases.

Results

Identification of ANKH as a candidate citrate exporter in human cellular senescence

Recently, ANKH has been identified as a plasma membrane exporter of citrate and to a lesser extent malate (30), two metabolites we found accumulated in the conditioned medium of both PEsen and IrrDSBsen senescent fibroblasts (23). Hence, we screened 3 fibroblast lines (NHOF-1, BJ and IMR90) for the expression of several plasma membrane transporters including ANKH in both confluent young (cell cycle arrested) and IrrDSBsen fibroblasts. The mitochondria/cytoplasm citrate exporter SLC25A1 (CiC), but not its plasma membrane form (pmCiC), was consistently upregulated in IrrDSBsen cells (Supplementary Figure 1). The same cells also showed an increase of *ANKH* expression in all three IrrDSBsen cultures (Figure 1A); an increase of between 8- and 9.6-fold relative to the confluent young quiescent controls (Figures 1B and 1C). Other plasma membrane transporters, the monocarboxylate transporters MCT1 (Supplementary Figure 1) and MCT4 (Supplementary Figure 1) showed either no upregulation (MCT1) or undetectable expression (MCT4); the neutral amino acid transporter ASCT2 was downregulated in all three IrrDSBsen lines (Supplementary Figure 1). We next examined whether *ANKH* expression was upregulated in senescent fibroblasts at the mRNA level. In IrrDSBsen NHOF-1 cells this was the case, as assessed by two *ANKH* primer sets (Figure 1D and 1E). $P16^{INK4A}$ was not generally elevated in NHOF-1 cells upon senescence (Figure 1F), but another senescence effector $p21^{WAF}$showed a strong trend for elevation in parallel to *ANKH* (Figure 1G).

The conditional knockdown of *ANKH* mRNA reduces EC in IrrDSBsen human fibroblasts.

To evaluate whether *ANKH* was a mediator of EC in senescent fibroblasts we transduced NHOF-1 fibroblasts with three inducible shRNA vectors targeted against *ANKH* and a non-targeting (NT) control. The results confirmed our previously published data that EC was 4-fold higher in the IrrDSBsen fibroblast conditioned medium than in the growing controls. Inducible shRNA knockdown of *ANKH* inhibited *ANKH* mRNA expression from between 46% and 52% in growing NHOF-1 cells following induction by doxycyclin (DOX; P 0.001 to 0.02) but did not reduce

EC levels significantly compared to the NT vector following induction by DOX (P =0.47 by the Welch's T test; Figure 1H), due to the very low levels of EC in the growing control group and a very low outlier in the NT group.. However, the difference between the DOX-induced and control shRNA groups was highly significant (P = 0.005). The same vectors reduced *ANKH* mRNA expression from between 31% and 59% in IrrDSBsen in NHOF-1 cells and EC was reduced by between 24 and 28% by all three shRNA vectors relative to the NT vector following induction by DOX (P = 0.03) and was reduced by 12 % (vector #2500) and 27% relative to the non-induced controls (P = 0.025). There was no significant effect of DOX on either *ANKH* mRNA or EC in the NT controls, EC in the medium blanks or the cell counts in any of the experimental groups. There was also no significant effect of the shRNA vectors on $p16^{INK4A}$ and $p21^{WAF}$ mRNA levels or SA-βGal relative to the NT controls. Although the effect of shRNA knockdown on EC was small it was significant in IrrDSBsen cells and given the modest level of *ANKH* mRNA knockdown the data indicate that *ANKH* at least partially mediates EC accumulation following fibroblast senescence.

***ANKH* mRNA is upregulated in parallel with senescence markers in PEsen human fibroblasts and is downregulated by the canonical function of telomerase.**

Next, we tested whether *ANKH* was upregulated in PEsen human fibroblasts in parallel with senescence markers and showed that this is indeed the case in NHOF-1 cells (Figure 2A and 2B); $P16^{INK4A}$ (Figure 2C), $p21^{WAF1}$ (Figure 2D) and SA-βGal (Figure 2E) are strongly upregulated in the same cells. Comparable results were obtained with PEsen BJ cells (Supplementary Figure 2A-E), except that $p16^{INK4A}$ was not upregulated ((Supplementary Figure 2C).

We have already reported that the canonical function of telomerase reduces the accumulation of EC in parallel with bypassing senescence, so we next considered whether the transduction of NHOF-1 and BJ cells with *TERT,* but not the non-canonical variant *TERT-HA* (34) or the dominant-negative (catalytically dead in fibroblasts) mutant *DNTERT* (35), regulated the

expression of *ANKH*. The results showed that in three independent NHOF-1 cultures and one BJ culture (Figure 2E, F; Supplementary Figure 2F, 2G) *TERT* expression reduced *ANKH* expression relative to the PEsen PURO controls. This occurred in parallel with $p16^{INK4A}$ (Figure 2H), $p21^{WAF1}$ (Figure 2I) and SA-βGal (Figure 2J-L; Supplementary Figure 2H). The *TERT-HA* and *DNTERT* controls, which fail to elongate telomeres (35, 36), did not reduce *ANKH* transcript levels or any senescence marker in either NHOF-1 (Figure 2) or BJ cells (Supplementary Figure 2). All *TERT* constructs were expressed in late passage NHOF-1 (Supplementary Figure 3A) and BJ cells (Supplementary Figure 3B). Only *TERT* increased telomerase activity in NHOF-1 cells (Supplementary Figure 3C), and only *TERT* and *TERT-HA* increased telomerase activity in BJ cells (Supplementary Figure 3D), as previously reported (34).

***ANKH* mRNA and EC are regulated by the p38 mitogen-activated kinase, Mitogen-activated protein kinase-activated protein kinase2/3 and the associated axis, but not by the Ataxia Telangiectasia Mutated kinase.**

We have previously reported that the kinetics of EC upregulation following the induction of IrrDSBsen are similar to that reported for the SASP and in particular, interleukin-6 (IL-6) (24). As p38 mitogen-activated kinase (p38MAPK)*(37)*, Mitogen-activated protein kinase-activated protein kinase (MK2/3) *(38)* and Ataxia Telangiectasia Mutated (ATM (39)) regulate the interleukins of the SASP, we tested whether pharmacological inhibition of these kinases would regulate EC and *ANKH*. Figure 3 shows the effect of the p38MAPK and MK2/3 inhibitors, SB203580 and PF-3633022 respectively, on young growing NHOF-1 and the same cells induced to senesce after the induction of IrrDSBsen. As reported previously, EC increased about 3-fold following IrrDSBsen and showed a trend for reduction with both drugs in both growing and IrrDSBsen groups, but the data were variable (Figure 3A). When the data was normalised to the controls for each experiment (Figure 3B) SB203580 showed a highly significant reduction of EC in IrrDSBsen cells, but not growing cells, and PF-3633022 inhibited EC significantly in both

growing and IrrDSBsen groups. Taken together the data shows that EC is regulated by both p38MAPK and MK2/3.

Next, we evaluated the effect of SB203580 and PF-3633022, as well as the *ATM* kinase inhibitor KU55933, on *ANKH* mRNA expression and senescence markers $p16^{INK4A}$ and $p21^{WAF1}$ over a larger dose range in both IrrDSBsen BJ (Figure 3C-G) and NHOF-1 cells (Figure 3H-L). The data showed that in both BJ and NHOF-1, SB203580 (between 1 and 10 µM) inhibited *ANKH* expression when assayed by both *ANKH* primer sets (*ANKH1* and *ANKH2*); PF-3633022 inhibited *ANKH* expression between 1 and 2.5 µM, although this was clearer with primer set *ANKH*1. The biphasic response of human fibroblasts to PF-3633022 regarding IL-6 secretion has been documented previously (40) and the effect on *ANKH* mRNA expression was similar. KU55933 did not affect *ANKH* expression over this period. The above doses of the inhibitors did not consistently affect the expression of $p16^{INK4A}$ or $p21^{WAF1}$, but 10 µM SB-203580 did reduce $p16^{INK4A}$ expression in NHOF-1 cells (Figure 3I) and PF-3633022 reduced $p21^{WAF1}$ expression in BJ cells at 1-10 µM (Figure 3F) and at 10 µM in NHOF-1 (Figure 3J). None of the inhibitors affected the level of senescence as assessed by the SA-βGal assay over the 3-day period of incubation in either BJ or NHOF-1 cells (Figure 3G and 3L).

Taken together our data shows that EC in IrrDSBsen cells is regulated in parallel with IL-6 and *ANKH* by p38MAPK and MK2/3 independently of cell cycle arrest and the senescence phenotype, but not by the *ATM* kinase.

To evaluate the effect of SB203580 and KU55933 on EC and IL-6 more thoroughly we exposed both growing and IrrDSBsen BJ cells to the drugs for 8 days individually and in combination. KU55933 alone had no effect on growing BJ cells but SB203580, either alone or in combination with KU55933 dramatically increased proliferation rate (Supplementary Figure 4A), reduced cell volume (Supplementary Figure 4B) and decreased SA-βGal (Supplementary Figure 4C), in line with previous reports that inhibiting p38MAPK antagonises cellular senescence (41). SB203580 and KU55933, but not KU55933 alone, also dramatically decreased EC

(Supplementary Figure 4D) and the same combinations had similar effects in IrrDSBsen cells (Supplementary Figure 4D), which are likely due to SB203580 alone (see above). The same combinations did not affect IL-6 levels in growing BJ cells. However, KU55933 alone had a dramatic effect on IrrDSBsen cells, causing a many-fold induction in secreted IL-6 and this effect was almost ablated by SB203580 suggesting that the inhibition of ATM in senescent cells exacerbates signaling through p38MAPK to increase IL-6 under the conditions described here (Supplementary Figure 4E). Taken together these data sets also highlight the fact that EC and IL-6 are independently regulated in senescent cells, which is further supported by data below.

EC and *ANKH* are not suppressed by physiological levels of steroids and are regulated independently from interleukin-6 in IrrDSBsen human fibroblasts.

It has been reported that both cortisol (hydrocortisone – HC) and corticosterone (CST) within the physiological range suppress many components of the SASP, including IL-6 (42). This may explain why SASP factors are not that high in human plasma in clinical trials of senolytic drugs (43), during human chronological ageing (44) or in the telomeropathy DC (25). We therefore tested the effect of HC and CST on EC, secreted IL-6 (42) and *ANKH* expression over an 8-day period. In IrrDSBsen BJ cells IL-6 is significantly reduced by HC and CST, as previously reported by others in a different setting (42), but EC is not (Figures 4A-4C). This supports the argument that EC and IL-6 are regulated independently. Interestingly, *ANKH* expression tended to be increased, especially with high doses of HC, rather than decreased (Figure 4D and 4E); there was no significant effect on $p16^{INK4A}$ (Figure 4F), $p21^{WAF}$ (Figure 4G) or SA-βGal (Figure 4H) and so the steroid effects on IL-6 were independent of senescence. Comparable results were obtained with NHOF-1 cells (Supplementary Figure 5).

Next, we tested the effect of the SASP regulator interleukin-1 alpha (IL-1α), which was reported to positively regulate IL-6 (42), on EC, secreted IL-6 and *ANKH* expression in BJ cells. IL-1α strongly stimulated the secretion of IL-6, an effect that was antagonised by HC, whereas

the effect on EC was the reverse. In this separate set of experiments, HC alone also inhibited IL-6 secretion (Supplementary Figure 6A) but had no effect on EC (Supplementary Figure 6B).

Finally, we tested another regulator of IL-6, sodium butyrate (NaB), which had been reported to induce secreted IL-6 independently of DNA double strand breaks, or senescence (45). Again, the data showed that in BJ cells and two oral fibroblast lines (NHOF-2 and NHOF-7) a four-day treatment of the cells with 1-4 mM NaB inhibited cell proliferation (Supplementary Figure 7A), caused cell flattening, increased cell volume and induced IL-6 secretion (Supplementary Figure 7B), without significantly affecting histone acetylation (H3K27ac) (Supplementary Figure 7C) and collagen (Supplementary Figure 7D). 53BP1 levels were slightly increased in NHOF-1 and NHOF-7 at 1mM NaB (Supplementary Figure 7E) and SA-βGal levels were increased in BJ cells (Supplementary Figure 7F). In contrast, $p16^{INK4A}$ (Supplementary Figure 7G) or $p21^{WAF1}$ (Supplementary Figure 7H) mRNA expression was not increased. In all cell lines, EC was modestly and insignificantly induced over this time frame, and not as high as in IrrDSBsen cells (Supplementary Figure 7I and Supplementary Figure 7J). In BJ cells, *ANKH* expression was, if anything, reduced (Supplementary Figure 7K; Supplementary Figure 7L).

These results confirm the association between EC and *ANKH* expression and the independent regulation of EC from IL-1α and IL-6.

IL-1α inhibits the production of EC and *ANKH* expression in proliferating human fibroblasts.

Under the conditions described here, IL1α actually stimulated BJ proliferation (Figure 5A) in parallel with a strong induction of secreted IL-6 (Figure 5B), as previously reported (42), but reduced EC (Figure 5C) in parallel with *ANKH* expression (Figure 5D and 5E) whilst having a minimal effect on $p16^{INK4A}$ (Figure 5F), $p21^{WAF}$ (Figure 5G) and SA-βGal (Figure 5H).

EC and hydrogen peroxide are negatively regulated by p53 independently of *ANKH* expression and are independent of the senescence effectors p16^{INK4A} and p21^{WAF1}.

To evaluate the effect of p53 on EC regulation we assessed a panel of human wild type, p53 null and p21^{WAF1} null embryonic lung fibroblasts (Loxo26WT, Loxo26 p53-/- and Loxo 26 p21^{WAF1} -/-). The results showed that whether growing, or following IrrDSBsen, Loxo26 p53-/- showed much higher levels of EC (Figure 6A) and hydrogen peroxide (Figure 6B) than their wild type and/ or p21^{WAF1} null counterparts. qPCR data confirmed the absence of p53 in the p53 -/- cells (Figure 6C) and showed that the p21^{WAF1} null Loxo26 cells had silenced p16^{INK4A} in addition to p21^{WAF} during passaging after receipt (Figures 6D and 6E). This means that EC regulation was independent of the senescence effectors p21^{WAF1} and p16^{INK4A}. However, EC was restrained by p53, analogous to its reported regulatory function on the SASP. (Figure 6A -see also reference (39))

The ability of p53 to restrain the accumulation of hydrogen peroxide (Figure 6B) was consistent with its reported antioxidant function (46) but under the conditions reported here there was no effect of p21^{WAF1} and p16^{INK4A} on hydrogen peroxide levels. To evaluate whether the restraining effect of p53 on EC was mediated by *ANKH,* we assessed the cell line panel for *ANKH* expression but found no consistent upregulation of *ANKH* in p53-/- Loxo26 cells or p21^{WAF1}/p16^{INK4A} -/- Loxo26 cells. (Figure 6F and 6G). There was no dramatic effect of p53 deletion on SA-βGal levels (Figure 6H) although p16^{INK4A} and p21^{WAF1} levels were significantly reduced (Figures 6D and 6E). We also evaluated the effect of inducible *TP53* shRNAs on the expression of *ANKH* mRNA and EC in growing NHOF-1 fibroblasts. shRNA #2 did reduce both *TP53* mRNA and that of its downstream target p21^{WAF} relative to the NT control by 59% and 53% respectively following induction by DOX (Figure 6I) but did not upregulate *ANKH* mRNA (Figure 6I) or EC in these cells (Figure 6J). *TP53* shRNA #2 significantly downregulated *ANKH* mRNA which may indicate a role for *TP53* in regulating *ANKH* independently of EC. Taken together the data suggests that *TP53* restrains EC independently of senescence or cell cycle inhibitors in

certain fibroblast lines, analogous to its effects on the SASP, but may do so independently of *ANKH* expression.

NaB induces senescence and EC accumulation independently of *ANKH* expression.

To evaluate the effect of senescence inducers other than those mediated by IrrDSBs or short telomeres, we assessed the ability of NaB to induce EC and senescence in the Loxo26 panel and $p21^{WAF1}$/$p16^{INK4A}$. We found that EC was elevated in the wild type cells following 3 weeks of 0.5 mM NaB treatment, but not in BJ cells (Figure 7A). This NaB effect was dependent on p53 and $p21^{WAF1}$/$p16^{INK4A}$. We then evaluated whether the effect on EC was associated with *ANKH* expression. We treated the Loxo26 panel, NHOF-1, BJ and IMR90 cells for 17 days and observed the classical senescence effect of cell flattening, increased cell size, increased $p16^{INK4A}$ (Figure 7B) and $p21^{WAF1}$ (Figure 7C) expression and in BJ and Loxo26 cells, increased SA-βGal (Figure 7D). However, despite inducing features of senescence NaB did not induce *ANKH* expression in BJ, NHOF-1 or Loxo26, and only did so in IMR90 at high doses (Figures 7E and 7F). This indicates that the induction of EC by NaB-induced senescence is variable between different fibroblast lines but is not mediated by *ANKH* induction.

Transforming growth factor β (TGFβ) induces *ANKH* expression prior to inducing senescence.

TGFβ will induce reversible cell cycle arrest in many cell types (47). The TGFβ family has also been implicated in the transfer of the senescence phenotype between cells (48). To examine the effect of TGFβ on *ANKH* expression and senescence we treated the cells for 4 days with 1 - 8 ng/ml of TGFβ1 in 4 mM HCl (Figure 8). The data showed that TGFβ1 significantly induced *ANKH* in NHOF-1 at low doses (Figure 8A and 8B) and showed a trend for induction in BJ cells (Figure 8A, 8B) in parallel with increased $p16^{INK4A}$ (Figure 8C) and $p21^{WAF1}$ (Figure 8D) expression. However, there was no evidence of senescence as assessed by SA-βGal (Figure 8E). These data indicate that TGFβ1 mediates *ANKH* expression in parallel with fibroblast activation prior to, or independently from senescence (49). Next, to test the role of the TGFβ family members in

regulating *ANKH* and senescence markers in established IrrDSBsen fibroblasts, we treated three lines of IrrDSBsen fibroblasts with two TGFβ type I receptor kinase inhibitors that had been reported to suppress the SASP (48). Figures 8F and 8G show that although the effect was small, both inhibitors significantly suppressed *ANKH* expression by 15-30% in all three lines without reversing the levels of $p16^{INK4A}$ (Figure 8H), $p21^{WAF}$ (Figure 8I) and SA-βGal (Figure 8J), at least in the case of inhibitor I. However, there was a significant reduction in $p21^{WAF}$ expression (Figure 8I) and a trend for SA-βGal reduction Figure 8J) in the case of inhibitor II. We conclude that the TGFβ family contributes to the regulation of *ANKH* in IrrDSBsen fibroblasts.

***ANKH* and EC are not upregulated in IrrDSBsen and PEsen keratinocytes or during keratinocyte differentiation, indicating cell type specificity in citrate export.**

As senescent mammary epithelial cells were reported not to shift their energy metabolism towards glycolysis and EC, albeit under very different culture conditions to those we used previously (27), we tested both EC accumulation and *ANKH* expression following IrrDSBsen in both 3T3-supported cultures and serum-free commercial media. We also tested the effect of ROCK inhibitor Y27632 (ROCKi) in the 3T3 system which has been reported to induce telomerase (50), thus replicating more accurately conditions in the epidermal basal layer (51). In all five epidermal keratinocyte lines IrrDSBsen resulted in a downregulation of EC relative to controls (Figure 9A) and the inclusion of ROCKi in the two 3T3-supported cultures did not change the result (Figure 9B). We also evaluated the effect of PEsen on *ANKH* mRNA expression in regular 0.09 mM calcium medium after 4 and 7 days after the induction of differentiation and stratification by 0.4 mM and 1.0 mM calcium chloride addition to serum-free keratinocyte medium. There was no consistent increase in *ANKH* (Figure 9C and Figure 9D), whilst $p16^{INK4A}$ (Figure 9E) and $p21^{WAF}$ (Figure 9F) mRNA increased as reported previously for $p16^{INK4A}$ protein following PEsen (52) in all conditions after 4 days, but not after the induction of differentiation (see below). We next addressed the role of differentiation and stratification on EC accumulation and *ANKH* expression in young cells by manipulating the calcium chloride concentration as above and monitoring the

extent of differentiation by involucrin (*IVL*) and keratin 9 (*K10*) expression. Figure 10 shows that in all five keratinocyte lines there was no consistent increase in EC (Figure 10 A, B) following the induction of differentiation. In four of the five lines, there was no increase in *ANKH* (Figure 10C, D), p16^{INK4A} (Figure 10E) or p21^{WAF} (Figure 10F) following the induction of differentiation as assessed by IVL (Figure 10G), or stratification by K10 (Figure 10H). Taken together our data shows there is no evidence that PEsen, IrrDSBsen or terminal differentiation regulates either EC or *ANKH* expression in human epidermal keratinocytes.

***ANKH/Ankh* mRNA is regulated in other types of IrrDSBsen and PEsen cell types relevant to aging and age-related disease and in chronologically aged mouse tissue.**

Next, we tested the relevance of *ANKH* upregulation in senescent cell types that are relevant to age-related disease in mice such as astrocytes (cognitive decline (53)), adipocytes (frailty (54) and type II diabetes (55)) and myoblasts (frailty (56)). We now show that *ANKH* was upregulated in adipocytes following confluence-induced adipocyte differentiation (Figure 11A, 11B) and senescence (as assessed by high p16^{INK11A} and p21^{WAF1}; Figure 11C and 11D); but not in PEsen or IrrDSBsen pre-adipocytes (Supplementary Figure 8). We, and others, have shown that long-term quiescence induced by confluence can induce senescence (57, 58).

Human myoblasts display markers of senescence and telomere-associated foci with increased chronological age (56). Human myoblasts cannot be immortalised by telomerase alone, but we were able to compare senescent and pre-senescent human myoblasts (HMC) transduced with the catalytic subunit of telomerase, *TERT*, (HMC *TERT* POOL or HMC *TERT* clone T2) and control (HMC) myoblasts. We were also able to compare these cells with a clone of *TERT*-transduced myoblasts that had spontaneously lost p16^{INK4A} (HMC *TERT* T15 (59)). In senescent *TERT*-expressing cells, *ANKH* was upregulated following PEsen (Supplementary Figure 9A, B) in parallel with p16^{INK4A} (Supplementary Figure 9C), p21^{WAF} (Supplementary Figure 9D) and SA-βGal (Supplementary Figure 9E). However, *ANKH* and all markers except p21^{WAF}

were strongly downregulated following immortalisation in HMC *TERT* T15. These data also show that *ANKH* is associated with senescence in human myoblasts.

Importantly, human astrocytes express *ANKH* (Figure 12A, 12B, 12G, 12H), which is significant as astrocytes are the source of citrate supply in the nervous system, although no candidate plasma membrane transporter has previously been identified (60). Our data suggests that ANKH is a candidate for a citrate exporter in astrocytes. In addition, we now show that *ANKH* is over-expressed in parallel with SA-βGal, $p16^{INK4A}$and $p21^{WAF1}$ in both IrrDSBsen (Figure 12A-E), together with old and PEsen human astrocytes (Figure 12F-J). Upon PEsen the astrocytes became much flatter, lost their bipolar appearance, and increased in size (Figure 12N) compared to young astrocytes (Figure 12L). Several SASP cytokines were upregulated in PEsen astrocytes along with Complement Factor 3, indicative of astrocyte activation (Supplementary Figure 10).

***Ankh* is downregulated following mouse chronological ageing in parallel with senescence markers.**

To assess the role of *ANKH* (*Ankh*) in mouse chronological ageing, we examined the levels of the *Ankh* transcript in C57BL6 mouse tissues where body fluid levels of citrate have been reported to be elevated at advanced chronological age. Figures 13A and 13B show that *Ankh* is much more highly expressed in brain tissue than liver or kidney. In all three tissue types, there was a trend for decreased levels of *Ankh* transcript with chronological age, which was significant in liver (Figure 13A) and the brain (Figure 13B). Older liver and kidney tissues do show increased *Ink4a* and *itgb3* transcript levels (61) confirming the increased presence of senescent cells (61). As regards the brain, immunohistochemistry revealed increased levels of cells in older mouse tissues expressing p53, $p19^{ARF}$, $p21^{WAF1}$ (Figure 13C), $p16^{INK4A}$, and γH2AX/53BP1) double stained foci (Figure 13D). All aged brain cells (mainly microglia and neurons) and neurons alone, showed a trend for increased telomere-associated foci with age (Figure 13D). Older mice showed increased levels of the SASP cytokines IL-1β, and TNFα and reduced levels of IL-10 in brain tissue (Figure 13E) and increased IL-6, TNFα and CXCL1 in serum (Figure 13F). Images of the

immunostaining in Figures 13C and 13D are shown in Figure 14. These data argue against a role for *Ankh* in the upregulation of mouse EC following chronological age, at least under the conditions described here. However, the results are consistent with the repression of EC and *ANKH* by IL-1α in human fibroblasts and the elevated levels of cytokines in the aged mouse serum and tissues (61), including brain (Figure 13E).

Discussion

There is now considerable evidence that energy (3) and citrate uptake (9-13, 17) are important for both ageing and age-related disease. For example, we have previously reported that EC is regulated by the canonical function of telomerase *in vitro* and in a human disease showing telomere attrition, Dyskeratosis Congenita (DC), *in vivo* (25). This supports the hypothesis that senescent cell derived EC may contribute to ageing and age-related disease, but the mechanisms underlying EC export were still unclear.

We show here that EC and its plasma membrane transporter *ANKH,* but no other plasma membrane transporters are associated with fibroblast senescence and are independent of cell cycle arrest and cell size. However, the mitochondrial form of SLC25A1/mCiC, is upregulated in some senescent cells, consistent with increased flux of citrate from the mitochondria to the cytoplasm. We have established that *ANKH* was required for EC accumulation in human fibroblasts using shRNA- mediated knock down but *Ankh* null mice have low levels of plasma citrate (30). However, the accumulation of EC in senescent cells and the increased expression of *ANKH* was cell type specific as neither occurred following keratinocyte or pre-adipocyte PEsen or IrrDSBsen, or indeed following keratinocyte differentiation and stratification. However, increased expression of *ANKH* mRNA was observed in senescent astrocytes, differentiated adipocytes and myoblasts as well as fibroblasts, and the increase in plasma EC in DC where the telomeres of leukocytes and fibroblasts are short (25) implies that increased *ANKH* and EC are common to many cell types involved in ageing. We previously established that the canonical

function of telomerase downregulated regulated EC in parallel with senescence (25) and we have now established that *ANKH* is similarly regulated.

As the kinetics of EC accumulation closely parallel that of the expression of IL-6 and other SASP proteins, we investigated the pathways reported to regulate IL-6 to test whether the same pathways also regulate EC. *p38MAPK* and its downstream kinase, MK2/3, were required for EC and *ANKH* transcript accumulation in established senescent cells, independently of cell size and cell cycle arrest under the culture conditions we used, although the effect was slightly less marked than that on IL-6. As p38MAPK is activated in numerous types of senescent cells, including astrocytes (62), these results suggested EC may also accumulate outside these cell types. As MK2/3 links the mTOR pathway and autophagy with the inflammasome(63), our results indicate that MK2/3 would be a promising drug target for suppressing both SASP cytokines (40) and EC. In support, MK2/3 inhibitors have been shown to ameliorate glucose homeostasis and enhance insulin signalling in obese insulin-resistant mice by a mechanism that is additive to the lead T2D drug, metformin (64).

TGF-β did induce *ANKH* expression in some fibroblast types in parallel with senescence markers, though not all. However, as the TGF-β family was previously reported to spread the senescence phenotype in a paracrine fashion (48), we tested whether pharmacologically inhibiting the TGF-β type 1 receptor kinase could downregulate *ANKH* in established IrrDSBsen fibroblasts. We found that this was the case, although the effect was small and not associated with the reversal of senescence markers.

Taken together our data suggests that EC accumulation via ANKH is limited to PEsen and IrrDSBsen and perhaps by TGF-β in certain cell types, although the last of this needs further investigation.

p53 which is known to restrain IL-6 in senescent pathways (37) also appeared to restrain EC, but this varied with cell type was independent of senescence and only partially associated with *ANKH* transcription.

In addition, the histone deacetylase inhibitor NaB induced a large increase in cell size and an increase in IL-6 in the absence of detectable IrrDSBs or senescence as reported by others (45), but did not induce significant levels of EC within 4 days. Furthermore, although longer-term NaB treatments induced senescence and in some instances EC accumulation, this was independent of *ANKH* induction, and so *ANKH* does not mediate all forms of EC accumulation following senescence.

Of further significance, we found that whilst the established orchestrator of the senescence-associated inflammasome, IL-1α(48), induced high levels of IL-6 as reported(42, 48) and its steroid inhibitors restrained it(42), these manipulations had no effect on EC or *ANKH* in established senescent and proliferating cells. This last observation suggests that EC accumulation and *ANKH* are regulated independently from IL-6 and are not merely a consequence of the inflammasome or inflammation, the latter of which is known to cause senescence and telomere dysfunction(65). In addition, IL-1α increased proliferation and reduced both EC and *ANKH* expression in the absence of any marked effect on senescence markers, whilst at the same time increasing IL-6 secretion. These data further underline the differential regulation of EC and IL-6 secretion despite their similar kinetics and common regulation by the p38MAPK, MK2/3 and TGF-β pathways.

There was no evidence for an increase in *Ankh* transcript in three mouse tissues with chronological age, despite reported evidence for EC accumulation in several mouse biofluids with age. This data suggests that *Ankh* does not mediate EC accumulation in mice(7, 8) but is consistent with *ANKH* and EC downregulation by IL-1α in human fibroblasts and with the upregulation of mouse SASP cytokines in the aged mouse brain, as in both situations inflammatory cytokines such as IL-6 are elevated. However, there is considerable evidence that plasma membrane transport in mice and humans is significantly different (14, 66) and the effect of citrate on organismal lifespan and health span even in mice may be dependent on diet and/or the specificity of uptake (11, 12, 14). Furthermore, the ability of aged human plasma to induce

senescence and inflammatory cytokines is much less than aged mouse plasma and interestingly only works in cell types such as kidney epithelium (67) that can import citrate via SLC13A2 (25) .

The role of *ANKH* in age-related disease in humans has yet to be determined, but genome-wide analysis has linked it with a predisposition to Alzheimer's disease (AD)(33);this is interesting given that we have shown that *ANKH* is upregulated in PEsen and IrrDSBsen astrocytes, which in turn are instrumental for AD development in mouse models (68). However, we observed a downregulation of *Ankh* in aged mouse brain tissue, mainly in neurons and microglial cells. Therefore, it is also possible that the link of *ANKH* to AD in humans (33) is also linked to its downregulation, as the associated single nucleotide polymorphism (rs112403360) is a non-coding intronic variant, so it is currently impossible to deduce how it pre-disposes to AD and the cell types in which it operates. However, cognitively healthy centenarians are enriched for the protective allele of rs112403360 and this has been suggested to be linked to its known role in bone and vascular health (69). However, increased *ANKH* function could also benefit citrate supply to the brain. Significantly, loss of function mutations in *SLC13A5* in humans result in neonatal epilepsy and injection of citrate into the brain can induce seizures (reviewed in (70)), so citrate levels need to be tightly regulated, and too little citrate or too much may be pathogenic.

There is considerable evidence that both senescent cells and plasma citrate contribute to several age-related diseases (reviewed in (6)). Citrate regulates the inflammatory elements of the SASP such as IL-6 (71, 72) and conversely IL-6 can upregulate citrate import in the liver by upregulating SLC13A5/INDY, albeit at doses one thousand times higher than those found in human plasma(73).

Based on our new results and the reports of others we propose a hypothesis that EC and IL-6 released by senescent cells may collaborate to induce some age-related diseases but may antagonise one another in others. Moreover, citrate may be just as important as glucose or fructose uptake in mediating the well-known effects of caloric restriction(3), especially as other reports have shown that citrate and sucrose in concert induce pre-insulin resistance in mice (72).

ANKH itself may not be a suitable drug target due to the reported deleterious effects of its dysfunction in both mice and humans (30). Whilst senolytic drugs would likely counter senescent cell-derived IL-6 and EC, our data showing that *Ankh* is downregulated in the aged mouse brain may be concerning for this approach, since citrate is essential for normal neuronal function.

However, citrate also enters the system through the diet, where it enters certain cells via the citrate importer *SLC13A5/INDY,* and in cancer cells via pmCiC(6). Import of citrate from the diet also might on the one hand explain why senolytic drugs slow, rather than block (1, 74), age-related disease and on the other hand, why it might improve the health span of mice fed on a high fat diet (11). Citrate import from the diet might compensate for the loss of citrate supplied by senescent cells such as astrocytes when such cells are removed by genetic or pharmacological manipulation(68).

Nevertheless, the citrate importer SLC13A5/INDY is an established drug target (14, 75) and our data suggest that SASP inhibitors (48), telomerase activators (76-78) and SLC13A5/INDY inhibitors (14) may have potential in the treatment of age-related pathologies by regulating citrate metabolism.

Conclusions and future directions.

In summary, our new data identifying that the novel citrate plasma membrane exporter *ANKH* is upregulated in a variety of senescent cell types relevant to ageing and its regulation by established drug targets, informs on how countering the deleterious effects of senescent cells and telomere attrition might be addressed in the future. However, as *ANKH* and citrate may have opposing effects in humans and mice as well as in different ageing tissues, depending on dietary factors (9-13), further research will be necessary to exploit these observations, especially in human tissues and organoids.

Limitations of the study.

We have demonstrated a link between *ANKH* and EC upregulation in senescent human cells *in vitro* and offered a potential explanation for the downregulation of *Ankh* in aged mouse brain. However, it remains to be demonstrated that astrocyte Ankh mediates the supply of EC to neurones and that its reduction mediates neurodegenerative pathologies such as Alzheimer's disease. This could be addressed by targeted knockout of *Ankh* in astrocytes in future studies.

Materials and Methods

Cell culture.

Cells.

BJ cells at 16 mean population doublings (MPDs) were a generous gift from Professor Woodring Wright of Southwestern University, Houston, Texas, USA and used at between 22 and 25 MPDs. Later passage BJ cells were obtained from the American Type Culture collection and passaged until senescent (PEsen). Normal human oral fibroblast lines NHOF-1, NHOF-2 and NHOF-7 cells were derived from explant cultures of normal oral mucosa and used at early passage between 18 and 22 MPDs and NHOF-1 was serially passaged until PEsen at between 65 and 70 MPDs (23). IMR90 cells at early passage were used between 1.9 and 15 MPDs after receipt. Late passage IMR90 cells were obtained from the American Type Culture collection at 28 MPDs and passaged until PEsen at between 58 and 60 MPDs.

Cells were cultured in DMEM supplemented with penicillin and streptomycin antibiotics to a concentration of 50 U/mL and L-glutamine to a concentration of 2 mM, containing 10% vol/vol fetal bovine serum at 37°C in an atmosphere of 10% CO_2/90% air. Flasks were kept at roughly 80% confluence, and medium was replenished every 3-4 days. Once cells became more than 80% confluent, or were needed for an experiment, they were washed once with warm (37°C) PBS containing 0.02% weight/vol EDTA before being incubated for 5 minutes with PBS containing 0.1% weight/vol trypsin and 0.01% weight/vol EDTA (1mL/10cm^2 dish). Following cell detachment, the trypsin was neutralized by the addition of serum containing media (3 mL media for every 1 mL trypsin solution), and cells were counted manually using a haemocytometer to enable calculation of the cumulative MPDs (MPDs). MPDs were used throughout the study as a measure of chronological age and were calculated using the formula: MPDs = 3.32((log10cell number yield) -(log10cell number input) (58).

Mycoplasma testing.

NHOF-1 was originally evaluated for mycoplasma using MycoFluor mycoplasma detection kit and found to be negative. Conditioned media both BJ and NHOF-1 cell line panels were evaluated for mycoplasma using a Lonza MycoAlert™ Mycoplasma Detection Kit and found to be negative.

Astrocyte Culture.

Human astrocytes were obtained from ScienCell Research Laboratories and cultured in astrocyte growth medium (ScienCell Research Laboratories, AM, Cat. #1801) supplemented with 2% vol/vol foetal bovine serum (Cat. #0010), 1% vol/vol Astrocyte Growth Supplement (AGS, Cat. #1852) and 1% vol/vol of penicillin/streptomycin solution (Cat. #0503).

Upon thawing, the ampoules from liquid nitrogen or subculturing the astrocytes were plated on poly-L-lysine-coated culture vessels. Vessels were pre-treated by adding 2 µg/cm^2, (10 mL of sterile water to a T-75 flask plus 15 µL of poly-L-lysine stock solution (10 mg/mL, Cat. #0413) or the equivalent thereof) to the appropriate culture vessel. The vessels were incubated at 37°C overnight and washed twice with sterile double distilled water before use. The cells were disaggregated as above when around 50% confluent and replated at around 1 x10^5 cells per T25 flask before use in experiments. The cells were maintained in an atmosphere of 5% CO_2/95% air.

The cmpds and the state of senescence PEsen and IrrDSBsen was analysed as indicted above.

Adipocyte Culture.

Human sub-cutaneous adipocytes were obtained from Cell Applications Inc. and cultured in pre-adipocyte growth medium (Cell Applications Inc. Cat# K811-500) supplemented with 5% vol/vol foetal bovine serum, 0.4% vol/vol endothelial cell growth supplement, 10 ng/mL recombinant epidermal growth factor, 1µg/mL hydrocortisone and 1% vol/vol and penicillin and streptomycin). The cells were disaggregated as above when around 50% confluent and replated

at around 1 x10^5 cells per T25 flask before use in experiments. The cells were maintained in an atmosphere of 5% CO_2/95% air.

The cmpds and the state of senescence PEsen and IrrDSBsen was analysed as indicted above.

Induction of adipocyte Differentiation.

To induce differentiation the cells were grown plated at 4.4 x 10^5 per cm to reach confluence and maintained in Cell Applications adipocyte differentiation medium (Sigma Aldrich Cat# 811D-250) for 15 days but were not starved as this might have affected cellular senescence and citrate metabolism.

Oil Red staining.

Adipocytes and pre-adipocytes were stained with Oil Red O using a commercial kit from Biovision (Cat# K580-42) and the intensity of staining semi-quantified by measuring the absorbance. After staining with hematoxylin and washing with distilled water, the cells were washed an additional three times with 60% isopropanol (5 min each time with gentle rocking). The Oil Red O stain was then extracted with 100% isopropanol for 5 min with gentle rocking (250 µL per well) 80% of extraction volume was used to measure. 100% isopropanol was used as a background control and subtracted from the background reading. Absorbance was read at 492 nm using a CLARIOstar plate reader (BMG LABTECH).

Keratinocyte culture.

The normal human epidermal keratinocytes were either obtained commercially from two pools of newborn foreskins each consisting of 3-6 donors (NHEK92 and NHEK131) 12332-011, Invitrogen, Renfewshire, UK - now Thermo Fisher Scientific) at MPD 0 or derived from juvenile skin from behind the ear (HEK124, HEK125 and HEK127 (52, 79)).

The cells were cultivated either using lethally irradiated 3T3 feeders as described previously(80) or in keratinocyte growth medium (KGM) containing 0.09 mM calcium chloride with reduced levels of bovine pituitary extract (12.5µg/mL) and epidermal growth factor (0.2 ng/mL) as

described by others(81). To induce terminal differentiation and cornification calcium chloride (300 mM Clonectics from Lonza Bioscience, Slough, UK) was added to a final concentration of 0.4 mM and 1.0 mM, respectively. Expression of involucrin and keratin 10 were used to monitor the level of differentiation.

Alternatively, for some experiments, keratinocytes were cultured in Dulbecco's Modified Eagles Medium (DMEM) containing 10% vol/vol fetal bovine serum (FBS –Hyclone fetal clone II) supplemented with 0.4µg/mL hydrocortisone, 2 mM glutamine ((GE Healthcare, PAA Laboratories GmbH, Austria) and antibiotics (streptomycin 50 U/ml Penicillin and 50 µg/mL streptomycin, Sigma, Poole, Dorset, UK) in an atmosphere of 10% CO_2/90% air. Keratinocytes were sub-cultured once weekly at a density of 1 x 10^5 cells per 9 cm plate to prohibit confluence.

In some additional experiments, keratinocytes were conditionally immortalised by the addition of the Rho kinase inhibitor Y27632 as described (80) maintaining telomerase levels analogous to conditions in the squamous basal layer.

The induction of senescence by ionizing radiation (IrrDSBsen).

Fibroblasts, keratinocytes astrocytes and adipocytes were irradiated in suspension with 10Gy of γrays from a Cs source at a dose rate of 1.4 Gy/min (23) or in later experiments with 10 Gy of X rays at a dose rate of of 3.6 Gy/min to induce irreparable DNA double strand breaks. The cells were left between 0 and 20 days in culture before analysis. Where indicated the keratinocytes were irradiated with γ rays in situ following removal of the 3T3 feeder cells with EDTA and vigorous pipetting as described(80). 3T3 feeder cells were irradiated with 60 Gy of either γ- or X rays as indicated above(80).

Experimental design and drug treatment.

Cells were seeded in such a way as to ensure that the density of both senescent and growing controls were similar although to induce short-term confluence higher numbers of cells

were seeded to ensure short-term reversible growth arrest, and the numbers of senescent cells seeded to match the level of confluence where indicated.

Cells were seeded for 3 to 5 days prior to medium changing for 16 h before lysis or collection of conditioned media. Except for the long-term NaB experiments all drugs, growth factors, cytokines and inhibitors were added for the indicated time and during the final 16 h prior to analysis. Controls were either culture medium with no additives or vehicle controls (ethanol or DMSO at 0.1% vol/vol)

For shRNA induction, cells were cultured in the indicated level of DOX for one week prior to setting up the experiment and for the entire experiment. Non-induced cells and DOX-induced cells expressing the non-targeting vectors served as controls.

Characterisation of senescent cells.

The cellular senescence status of the cells was confirmed through senescence-associated beta galactosidase (SA-βGal) activity using commercial kits (Biovision K-320-250 and later Generon senescence activity assay kit Cat# KA6035), which was measured again at the time at which the experiments were conducted. Briefly, the kits were brought to room temperature for 20 minutes. Following this, the cells were washed twice with calcium and magnesium-free phosphate buffered saline (PBS) fixed for 10 min and washed twice more before adding the SA-βGal reagent. The plates were then sealed with parafilm to prevent dehydration, covered in foil to protect from light and incubated at 37°C in a hot room or hotbox in an atmosphere of air (0.03% CO_2. Late passage IMR90 cells were used as a positive control.

Western blotting.

The following antibodies were used: pmCiC and mCiC (SLC25A1) rabbit polyclonal antibodies (82) were custom-made by GenScript Inc., ANKH (Rabbit VivaSystems, cat#OAAB06341), (MCT1 (rabbit Santa Cruz cat#sc-365501), MCT4 (goat Santa Cruz cat# sc-14930), Actin C-4 (mouse Santa Cruz cat# sc-47778), ASCT2 (rabbit Cell Signaling cat# 5345).

Briefly, cell extraction was performed to isolate proteins from confluent cultures. Cells were washed with PBS and extracted with 2× sodium dodecyl sulphate (SDS) Laemmli sample buffer (0.5 M Tris-Cl pH 6.8, 4% SDS, 20% glycerol; 10% (v/v) 2-mercaptoethanol was added after protein assay) immediately. DC Protein Assay (Bio-Rad, Hercules, CA, USA) was used to determine the protein concentration for each sample. use approx. 25 µg (10-30 µg) of protein was prepared with 5µL Laemmli Buffer, centrifuged at 15,000 rpm (20,000 g), boiled at 95°C for 5 min, spin down, centrifuged again and stored on ice.

The proteins were separated on 10% SDS polyacrylamide gels at 100V for 90 to 150 min, transferred to nitrocellulose filters (Whatman) in SDS running buffer and methanol at 100 V for 50-60 min. After blotting, the membrane was placed in 5% w/v-milk powder in Tris-buffered saline containing 10% w/v SDS, glycine, 0.1% vol/vol Tween 20 (TBS-T) on shaker for 1 h. Following blocking, the primary antibodies were diluted 1:1000 in TBS-T and 5% w/v/ milk powder and incubated at 4ºC overnight. The following day the membranes were washed twice for 15 min each in TBS-T with agitation. The membranes were then incubated with the appropriate secondary antibody at a dilution of 1:2500 in TBS-T and 5% w/v/ milk powder for 1 h at room temperature. The membranes were washed twice more for 15 min each in TBS-T with agitation before incubating with freshly prepared ECL for 2 min and developing with X-ray film developer in the dark and marking the molecular weight markers on the film. The membranes were washed with TBS-T as above before repeating with the loading control.

Retroviral infection of BJ and NHOF-1 cells.

pBABE retroviral vectors on the puromycin-resistant backbone expressing *TERT* and *TERT-HA* (36) or the empty vector were obtained from Addgene Europe, Teddington, Middlesex, UK. Retroviral vectors were transfected into Phoenix Amphotropic 293T cells (83) to create infectious amphotropic retrovirus in 48 h. The conditioned medium containing the retrovirus was filtered through a 0.45 µm filter to remove Phoenix A producer cells and then incubated with sub-confluent late passage NHOF-1 (45 MPDs) or BJ cells (65 MPDs) for a further 48 h without polybrene as

this is not recommended for the infection of normal cells. The infected and mock-infected NHOF-1 and BJ cells were then trypsinized and replated at a density of 5 x 10^5 cells per T75 flask and cultured for a further 48-72 h before adding 1 µg/mL of puromycin as a selecting agent. The puromycin was included in the medium until all the cells on the mock-infected plates had died and removed thereafter as selecting agents can reduce the replicative lifespan of normal cells (84). Re-introducing selection before analysis did not change the expression of the *TERT* transgenes. Cells were expanded in control medium lacking puromycin, cryopreserved and serially passaged when confluent at 1.5-3 x 103 cells per cm^2 until the control cells senesced. Medium was changed twice weekly.

Collection of conditioned medium.

Conditioned medium was collected after 24 h from the cells, centrifuged at 800 x g for 2 min, the supernatant removed and centrifuged again at 15,000 rpm for 2 min and the final supernatant snap frozen on an ethanol-dry ice bath for 15 min before storage at -80°C. Unconditioned medium was also prepared identically.

Real time measurement of telomerase activity.

Telomerase activity using qPCR was performed with a QuantStudio 7 Flex Real-Time PCR system using the TRAP protocol as described in (85). Briefly, pellets containing 1x10^6 cells were washed in cold 1X PBS (Gibco™, US), lysed and resuspended in 150 µL of TRAPeze® 1X CHAPS Lysis Buffer (Chemicon®, Merck Millipore). Protein concentration of the samples was determined using the CB-X Protein assay (G-Biosciences) according to manufacturer's guidelines. Primer sequences were as described in (86). For the qPCR-TRAP reaction, each sample consisted of: 12.5 µL *Power* SYBR® Green Master mix (Applied Biosystems™, US), TS primer (0.1µg, 100 ng/µL; Invitrogen ™, US), ACX primer (0.05 µg, 100ng/µL; Invitrogen ™, US). 250 ng of sample protein extract and nuclease-free water (Ambion, Invitrogen ™, US) was added to bring a total volume of 25 µL reaction then loaded into MicroAmp Optical 96 well plate (Applied Biosystems™, US). The PCR plate included a positive control (PC3-hTERT), a negative control

(PC3-hTERT protein boiled for 10 min to deactivate the telomerase enzyme) and a single standard curve, PC-3-hTERT protein extract for serially diluted ranging from 50 ng-500 ng. The TRAP PCR cycle started with an initial incubation at 25ºC for 20 min and amplification at 95ºC for 10 min, followed by 35 PCR cycles at 95ºC for 30 sec and 60ºC for 90 sec. PC-3-hTERT standard curve RQ values were used to calculate the telomerase activity of the unknown samples (RQ) and then results were converted to percentage and plotted in a bar graph using Prism.

***hTERT* mRNA analysis**

Extraction of RNA from cell lines/strains was conducted using TRI Reagent (Merck Life Sciences, Dorset UK) according to the manufacturer's instructions. Samples were then treated with deoxyribonuclease I (DNAse I, Invitrogen; Thermo Fisher Scientific, Inc.) to remove contaminating DNA from the RNA. 1 ug of DNAse 1-treated RNA was reverse-transcribed into first-strand cDNA using the High-Capacity cDNA Reverse Transcription kit (Applied Biosystems; Thermo Fisher Scientific, Inc.). The primer sequences and thermal cycling parameters used to quantify fully spliced *hTERT* (primer set E4-E5) and GAPDH (primer set E1-E3) was the same as described previously (87) using *Power* SYBR® Green Master mix (Applied Biosystems™, US). RQ data analysis was initially performed using the SDS 2.4 software (Applied Biosystems; Thermo Fisher Scientific, Inc.) then plotted as bar charts in Prism.

Targeted measurement of extracellular citrate by gas chromatography/mass spectroscopy (GC-MS).

Deuterated citrate (Citrate-d_4) was added to each sample to a final concentration of 0.1 mM as an internal standard. Metabolites were then extracted using cold methanol before being dried under vacuum desiccation. The samples were re-suspended in anhydrous pyridine containing the derivatisation agents methoxyamine hydrochloride followed by N-Methyl-N-trimethylsilyltrifluoroacetamide with 1% 2,2,2-Trifluoro-N-methyl-N-(trimethylsilyl)-acetamide and Chlorotrimethylsilane (MSTFA+1%TMCS). GCMS was performed in pulsed split less mode on a Hewlett Packard HP6890 series GC system with Agilent 6890 series injector and a 30 m x 250

µm capillary column (Agilent, model number 19091s-433HP5MS) using a flow rate of 1 mL/minute, and a Hewlett Packard 5973 mass selective detector. The acquisition was conducted in selective ion monitoring mode, with the m/z values 273, 347, 375 and 465 for citrate, and 276, 350, 378 and 469 for citrate-d_4. The dwell time for all these ions was 50ms.

Targeted measurement of extracellular citrate by liquid chromatography/mass spectroscopy (LC-MS).

We measured citrate using a targeted LC-MS-MS method with a mixed-mode UPLC chromatographic separation step for retention and discrimination of organic acids, including excellent discrimination of citrate from isocitrate. The media samples were diluted 10fold with cold methanol, and then diluted again 5fold with cold methanol containing an internal standard (1 µg / mL L-Phenyl-d_5-alanine (Sigma-Aldrich, 615870)). The mixture was vortexed at 6 °C for 20 minutes, and then centrifuged (17,000 g, 10 minutes, 4 °C). 490 µL aliquots of the supernatant were dried under reduced pressure and stored at -80 °C until analysis.

We then resuspended the dried samples in 50 µL of water containing the stable-isotope-labelled (SIL) standard $^{13}C_3$-citrate (Cambridge Isotope Laboratories, CLM-9876), and measured citrate essentially as described by Smith et al (88) with modification of the LC gradient. Specifically, the initial binary elution gradient was 0% B; 0.1 min: 0% B; 8.1 min: 25% B; 11.1 min: 95% B; 12.1 min: 95% B; 13 min: 0% B and 15 min: 0% B. The separation was performed using an Acquity Premier CSH Phenyl-Hexyl column (2.1 × 100 mm, 1.7 µm). The analysis was performed on a XEVO TQ-S (Waters UK) using negative ionization mode, with settings of capillary voltage, 1.5 kV; source offset, 50 V; desolvation temperature 500°C; source temperature, 150°C; desolvation gas flow, 1000 L/h; cone gas flow, 150 L/h; nebuliser gas 7.0 bar; collision gas, 0.15 mL/min. The transitions used in MS were detailed as follow: Citrate Q1 191.0197 *m/z* → Q3 111.1000 *m/z*, collision energy 12 V; Q1 191.0197 *m/z* → Q3 87.1000 m/z, collision energy 18 V and $^{13}C_3$ citrate Q1 194.0197 *m/z* → Q3 113.1000 *m/z*, collision energy 12 V; Q1 191.0197 m/z

→ Q3 87.1000 m/z, collision energy 18 V. All the transitions set a dwell time of 0.008 second and a cone voltage of 45 V.

We quantitated citrate against an authentic standard (Supelco) using a 6-point calibration curve (from 0.025 – 1 mg/l, run immediately before and after the samples), together with the SIL ratio. The results were checked against both water and method blanks.

Reverse transcription and quantitative PCR (RT-qPCR).

Cultured cells were lysed in lysis buffer and mRNA extraction was performed as per manufacturer's instruction using Dynabeads mRNA Direct kit #61012 (ThermoFisher, UK). Purified mRNA sample was then combined with qPCRBIO SyGreen 1-Step Go (PCR Biosystems, PB25.31-12) master mix and qPCR primers for one-step relative quantification of target genes and 2 reference genes using a 384-well format LightCycler 480 qPCR system (Roche) based on our previously published protocols (89-92) which are MIQE compliant (93). Briefly, thermocycling begins with 45ºC for 10 min for reverse transcription followed by 95ºC for 30 s prior to 45 cycles of amplification at 95ºC for 5 s, 60ºC for 5 s, 72ºC for 5 s, 78ºC for 1 s (data acquisition). A 'touch-down' annealing temperature intervention (66ºC starting temperature with a stepwise reduction of 0.6ºC/cycle; 8 cycles) was introduced prior to the amplification step to maximise primer specificity. Melting analysis (95ºC for 30 s, 75ºC for 30 s, 75-99ºC at a ramp rate of 0.57ºC/s) was performed at the end of qPCR amplification to validate single product amplification in each well. Relative quantification of mRNA transcripts was calculated based on an objective method using the second derivative maximum algorithm (94) (Roche). All target genes were normalised to two reference genes (HPRT1 and B2M) validated previously (90) to be amongst the most stable reference genes across a wide variety of primary human epithelial cells, dysplastic and squamous carcinoma cell lines, using the GeNorm algorithm (95). Relative expression data were then exported into Microsoft Excel for statistical data analysis. No template controls (NTC) were prepared by omitting tissue sample during RNA purification and eluates were used as NTCs for each qPCR run.

Human primer sequences

Gene	Sequence	Product size (bp)
B2M-F	AAGTGGGATCGAGACATGTAAG	70
B2M-R	GGAATTCATCCAATCCAAATGCG	
HPRT1-F	TGACACTGGCAAAACAATGCA	93
HPRT1-R	GGTCCTTTTCACCAGCAAGCT	
ANKH-F	ACCAAAGCCGTCCTGTGTA	112
ANKH-R	CCACATGGTGCAGTTTATTGA	
ANKH-2F	CGGCCTATTGTCAACCTCTTT	78
ANKH-2R	TGTCAAAATCGCCACTGC	
p16-F	TGCCCAACGCACCGAATAG	176
p16-R	CACCAGCGTGTCCAGGAAG	
p53-F	AGGCCTTGGAACTCAAGGAT	85
p53-R	CCCTTTTTGGACTTCAGGTG	
p21-F	TCACTGTCTTGTACCCTTGTGC	127
p21-R	GGCGTTTGGAGTGGTAGAAA	
IVL-F	TGCCTGAGCAAGAATGTGAG	83
IVL-R	TTCCTCATGCTGTTCCCAGT	
K10-F	AAACCATCGATGACCTTAAAAATC	134
K10-R	GCGCAGAGCTACCTCATTCT	
IL1A-F	TGCCCAAGATGAAGACCAACC	70
IL1A-R	ACTACCTGTGATGGTTTTGGGT	
IL1B-F	CCTCCAGGGACAGGATATGG	92

IL1B-R	CCAAGGCCACAGGTATTTTGTC	
IL6-F	AAGTCCTGATCCAGTTCCTGC	77
IL6-R	GGCATTTGTGGTTGGGTCAG	
CXCL1-F	AACCGAAGTCATAGCCACACT	117
CXCL1-R	TCTGGTCAGTTGGATTTGTCACT	
C3-F	GGGCGTGTTCGTGCTGAATA	78
C3-R	CCGATGTCTGCCTTCTCCAC	

The knock down of target genes by conditionally expressed short hairpin RNA (shRNA) constructs.

We used pre-prepared lentiviral particles to infect the indicted human cells from Horizon Discovery (SMARTvector Inducible Lentiviral shRNAs).

First, we identified promoter, which gave the best induction of shRNA based on either Green Fluorescent Protein (GFP) or Red Fluorescent Protein (RFP). We did this by utilizing the SMARTchoice inducible non-targeting control 4-Pack (Cat #VSC6847) and following the manufacturer's instructions. Based on these pilot experiments we identified the mouse cytomegalovirus promoter as giving the best induction and so proceeded to work with constructs on this backbone.

The indicated cells were infected with lentiviral particles in transduction medium (serum-free Dulbecco's Modified Eagle Medium (DMEM) High Glucose without L-Glut or Sodium Pyruvate at a multiplicity of infection of 0.3 virus particles per cell. The following day the cells were changed into regular culture medium and on day 3 trypsinised and plated at 1 x10^5 cells per T75 flask. After a further incubation time of 4 days 1 µg/ml puromycin was added until all the mock-infected cells were dead and then the puromycin was removed prior to expansion of the cell populations and cryopreservation. We used this protocol because culturing normal cells in selecting agents can reduce replicative lifespan.

The dose of doxycyclin hyclate (DOX; Thermo Scientific, Cat #ICN19895510) was optimized by measuring GFP or RFP fluorescence following 4 days of induction. The toxicity of DOX was estimated in parallel by the addition of MTT for 1 hour in serum-free DMEM followed by dissolving the cells in Dimethyl Sulphoxide (DMSO) and measurement of the absorbance at a wavelength of 570nm. The level of knockdown by each shRNA was monitored by qPCR as indicated below. To achieve maximum levels of knock down the induced cells were purged of low expressing cells by flow sorting for cells highly positive for GFP or RFP after induction with DOX.

The sequences of each shRNA targeting sequence are given below.

Target	Fluorochrome	Targeting Sequence
Non-targeting	mouse CMV turbo GFP	Cat#VSC6570
Non-targeting	mouse CMV turbo RFP	Cat#VSC6571
ANKH#1002	mouse CMV turbo GFP	Cat#V3SH7669-227064850 **GGCACCAAGAACCGGATCA**
ANKH#2500	mouse CMV turbo GFP	Cat#V3SH7669-230823352 **TGCTCCCCGAAGTCGATGG**
ANKH#5474	mouse CMV turbo GFP	Cat#V3SH7669-228017824 **TTTGAAGTCACTCATGGGA**
TP53#1	mouse CMV turbo RFP	Cat#V3SH7669-227164253 **CACACGCAAATTTCCTTCC**
TP53#2	mouse CMV turbo RFP	Cat#V3SH7669-225233423 **AGGCCCTTCTGTCTTGAAC**

TP53#3	mouse CMV turbo RFP	Cat#V3SH7669-225995888 **TATTTCATTAACCCTCACA**

Measurement of cellular reactive oxygen species (ROS)

$1x10^5$ adherent cells were incubated for 1 h with 1 mM (2', 7'-dichlorouoroscin Diacetate (H2DCFDA), catalog number 287810 from Calbiochem) in DMEM containing 10% vol/vol FBS. After trypsinisation as described previously, the cell suspension was centrifuged at 1000 rpm for 5 min. The cell pellet then was re-suspended in 500 mL 1xPBS at 37°C and the suspension was transferred to FACS tubes with 1 µL of DAPI added to enable cell viability counts. With the help of Dr Gary Warnes at the Blizard Flow Cytometry Core Facility, a Beckton Dickinson BD LSRII ow cytometer was used to detect cells that had sufficient ROS to oxidise the non-fluorescent product of H2DCFDA to the fluorescent 2', 7' {dichlorouorescein (DCF). DCF has excitation and emission spectra of 495 nm and 529 nm respectively. As a positive control, cells treated with 1 mM Tert-butylhydroperoxide (Luperox TBHP solution, 458139 lot#BCBG4467V Sigma Aldrich) for 2 h were used, with or without recovery time prior to the assay and as a negative control, cells treated with the antioxidant PBN (N-tert-butyl-a-phenylnitrone B7263, Sigma Aldrich) at 1 mM in DMEM containing 10% vol/vol FBS for 1 or 2 h before assay were used. Non-viable cells as determined by DAPI staining were excluded from the counts and cells within the gates of viable and positive for DCF were compared to cells within the gates of viable but negative for DCF.

Enzyme-Linked Immunosorbent Assay (ELISA)

To measure IL-6 in conditioned media a sandwich ELISA method (Quantikine® ELISA Immunoassay, R&D Systems, Abingdon, UK) was employed following the manufacturer's protocol. The detection limit for IL-6 was 3.13-300 pg/ml.

Source of reagents and kits

Cytokines and steroids

TGF beta 1 R&D Systems Cat# 240B-002; interleukin 1alpha recombinant Human IL-1 alpha/IL-1F1 R&D Systems Cat#: 200-LA; corticosterone Sigma Aldrich Cat# 27840; hydrocortisone hemisuccinate (cortisol) Sigma Aldrich Cat# H2270.

Pathway inhibitors

KU55933 R&D Systems Cat# 3544/10; SB203580 Tocris Chemical Company Cat#1202; PF-3644022 Tocris Chemical Company Cat#4279; TGFBR1 kinase inhibitor 1 LY-364947 Calbiochem 616451; TGFBR1 kinase inhibitor 2 Calbiochem 616452.

Kits

Human IL-6 Quantikine ELISA Kit R&D systems cat# D6050; senescence detection kit Biovision K320; Generon senescence activity assay kit Cat# KA6035; Oil Red O kit Biovision (Cat# K580-42).

Miscellaneous chemicals

2', 7'-dichlorouoroscin Diacetate (H2DCFDA), Cat# 287810 from Calbiochem).

Tert-butylhydroperoxide (Luperox TBHP solution, 458139 lot# BCBG4467V Sigma Aldrich).

N-tert-butyl-a-phenylnitrone Cat# B7263, Sigma Aldrich).

Puromycin Sigma Cat# P8833.

Calcium Chloride 300 mM solution Lonza Cat# CC-4202.

Sodium butyrate Sigma Aldrich Cat# B5887.

Trypsin (Worthington Biochemicals Cat# LS0033703.

Ethylenediaminetetraacetic acid (EDTA) Sigma Aldrich E5134.

Mouse experiments

The details and characterisation of the mouse liver and kidney tissues have been published previously (61).

Animals for the aged brain analysis.

The available strain for studying the role of ageing was C57BL/6, adult (8-10 weeks old) and aged (17 months old) male C57BL/6 mice, weighing 20-24 g at the start of the study (Janvier Laboratory, France). The Animal Welfare and Ethical Review Body, at Queen Mary University of London and the United Kingdom Home Office, following the EU Directive 2010/63/EU, approved all animal procedures.

Animal culling and sample collection

In order to collect tissue, animals were deeply anaesthetised using sodium pentobarbital (50 mg/kg) administered intraperitoneally (i.p.) in a volume of 0.5 mL/kg. Brain tissue and blood samples were collected from all animals. Animals were either perfused with phosphate-buffered saline (PBS) followed by 4% paraformaldehyde (PFA) for the analysis of the tissue by immunostaining, or with PBS only for the cytokine analysis that required fresh frozen tissue. Blood samples were collected in lithium heparin tubes and then centrifuged at 10,000 g for plasma separation. Plasma samples were stored at -80˚C for future analysis.

Immunostaining

All tissue staining was performed on 8 µm coronal brain sections cut between bregma -1.9 mm and -2.1 mm. Sections were deparaffinised in two washes xylene (10 min each) and then hydrated in a series of ethanol (EtOH) baths (100% EtOH, 100% EtOH, 90% EtOH and 70% EtOH, 5 min each) and two washes of PBS (5 min each). Then sections were treated with a heated antigen retrieval solution containing 10 mM citric buffer (pH 6.0) for 10 min in a microwave. After that, sections were blocked with 8% bovine serum albumin (BSA), 0.5% Tween-20 and 0.1% Triton X-100 in PBS overnight in a humidified chamber at 4˚C. On the next day, sections were washed twice in 0.5% Tween-20 and 0.1% Triton X-100 in PBS (PBS-TT) and then incubated with primary antibodies (Table 2.2) overnight in a humidified chamber at 4˚C. Markers were visualised using secondary goat-raised antibodies, which were labelled with either Alexa 488 or Alexa 555 (Invitrogen, United States; 1:250), and nuclei were visualised using Hoechst 33342

stain (Tocris Bioscience, United Kingdom; 1:500). Slides were mounted and cover-slipped using Vectashield fluorescent mounting medium (Vector Laboratories, United States).

Antibodies used.

Marker	Antibody full name	Species	Company	Product ID	Dilution
Anti-p53	Anti-tumour protein P53	Rabbit	Insight Biotechnology, United States	GTX102965	1:150
Anti-$p21^{Waf}$	Anti-cyclin-dependent kinase inhibitor 1	Rabbit	Invitrogen, United States	14-6715-81	1:150
Anti-$p16^{Ink4A}$	Anti-cyclin-dependent kinase inhibitor 2A	Rat	Abcam, United Kingdom	ab241543	1:150
Anti-$p19^{Arf}$	Anti-ARF tumour suppressor	Rat	Novus Biological, United States	NB200-169	1:150
Anti-γH2AX	Anti-phosphorylated H2A histone family member X	Mouse	Merck KGaA, Germany	05-636	1:500
Anti-53BP1	Anti-tumour suppressor p53-binding protein 1	Rabbit	Cambridge Bioscience, United Kingdom	A300-273A	1:1600

ImmunoFISH telomere associated foci (TAF) staining

ImmunoFISH staining was used to detect senescent cells. First, sections were deparaffinised in two washes of xylene (10 min each), washed in a gradient of ethanol (100% EtOH, 100% EtOH, 90% EtOH and 70% EtOH, 5 min each) and then in two changes of PBS (5 min each). After that, sections were treated with ice-cold (-20˚C) 70% ethanol for 20 min then

washed three times in PBS for 15 min. Next, sections were blocked with 8% BSA (Sigma-Aldrich, Saint Louis, United States), 0.5% Tween-20 (Sigma-Aldrich, Poole Dorset, United Kingdom) and 0.1% Triton X-100 (Sigma-Aldrich, Poole Dorset, United Kingdom) in PBS overnight at 4˚C in a humidified chamber. On the next day, sections were washed with PBS-TT for 5 min, then one or two primary antibodies were added and then left overnight at 4˚C in a humidified chamber. One of them was an anti-phospho-histone γH2A.X antibody (Cell Signalling Technology, Danvers, United State; 1:250) and the second was anti-NeuN (Merck Millipore, Burlington, United States; 1:250). On day 3, sections were washed in PBS-TT for 5 min twice then incubated with the secondary antibodies: biotinylated anti-rabbit IgG (Vector Laboratories, Burlingame, United States; 1:250) and Alexa Fluor 647 (Far red; Invitrogen, Carlsbad, United States; 1:250) for 1 h in a humidified chamber. After that, sections were washed in PBS-TT for 5 min three times, then incubated with DSC-Fluorescein (Vector Laboratories, Peterborough, United Kingdom, 1:500 in PBS) for 20 min. Later, sections were washed twice with PBS-TT, twice with PBS for 5 min, then treated with 4% PFA in PBS for 20 min. Next, sections were washed 3 times with PBS for 5 min followed by a dehydrating step using an ice-cold gradient of ethanol (70% EtOH, 90% EtOH, and 100% EtOH, 3 min each). Sections were air-dried and then treated with a hybridisation mix which contained 0.5 µg/mL (C3TA2)3-Cy3-labeled peptide nucleic acid (PNA) telomeric probe, 70% formamide, 12 mM Tris-HCl (pH 7.4), 5 mM KCl, 1 mM $MgCl_2$, 0.001% Triton X-100, and 2.5 mg/mL acetylated BSA. Sections were coverslipped and then incubated in the oven (82˚C) for 10 min. The hybridisation process was continued in a humidified chamber for two hours. Finally, sections were washed in 70% formamide/2xSSC for 10 min, twice in 2xSSC for 10 min, twice in PBS for 10 min then another change of PBS for 30 min. Slides were mounted using Vectashield fluorescent mounting medium with 4′,6-diamidino-2-phenylindole **(**DAPI) (Vector Laboratories, Burlingame, United States).

Quantification of IF and TAF signals

Four coronal sections were used per animal for each antibody staining; the sections were situated along the rostral-caudal axis, with a spacing of 0.1 mm between sections. Images were captured at x40 magnification using the In Cell Analyser 2200 (INCA2200) System (Cytiva, Marlborough, United States) for the markers: 8-oxo-dG, p53, $p19^{ARF}$, $p21^{WAF}$, and $p16^{INK4A}$. For the γH2AX.53BP1 signal overlap and TAF staining, fields used for the quantification were taken at x60 magnification using the In Cell Analyser 6000 (INCA6000) Confocal System (Cytiva, Marlborough, United States). A minimum number of 200 fields of view (FoV) were captured per animal covering all 4 sections, with a total of nuclei counts of at least 3 x 104 nuclei.

All quantitative analyses were conducted using the In Cell Developer Toolbox v1.9.2 (Cytiva, Marlborough, United States) and dedicated custom-made protocols were written for each marker evaluated, using the build-in parameters selection tools. A cell was considered positive for a marker when the fluorescent signal co-localised with a nucleus by at least a 95% overlap. Results were expressed as a percentage of the total nuclei detected.

Cytokine analysis

Brain samples

Snap-frozen brain tissue was used for cytokine analysis. 25 mg tissue was used from each sample, and the tissue was cut into small pieces on ice. The tissue fragments were suspended in lysate buffer (RIPA Buffer containing protease/phosphatase inhibitors) and then crushed with Pellet Pestle® (Sigma-Aldrich, United Kingdom). After that, samples were placed on rotating wheels and incubated for 20 min at 4°C. Next, samples were sonicated 3 times, 15 to 20 sec each, followed by centrifugation for 20 min at 10,000 g (4°C). Then, the supernatant was collected from each sample and used for the bicinchoninic acid (BCA) assay to measure protein concentration and subsequently cytokine concentrations.

For the BCA assay, the Pierce BCA protein assay kit (Invitrogen, Life Technologies Ltd, United Kingdom) was used to measure the concentration of protein extracted from brain tissue

and protocol followed manufacturer instruction. Samples were diluted with the supplied MSD solution, Diluent 41, to reach a concentration of 2.5 mg/µL which was the recommended protein concentration.

Plasma samples

Thawed plasma samples were diluted with the MSD supplied solution, Diluent 41, with a ratio of 1:3 before being used in the assay.

Running the experiment and data processing

Cytokine levels were measured in brain tissue and plasma samples using the V-PLEX proinflammatory panel 1 mouse kit, catalogue No. K15048D-1 (Meso Scale Diagnostics (MSD), United States), protocol followed manufacturer instructions and prepared plates were analyzed using MESO QuickPlex SQ 120MM (MSD, United States).

Mouse qPCR and primer sequences.

The qPCR was carried out for the mouse Ankh gene in the same way as for the human ANKH gene. The mouse primers are shown below.

Gene	Sequence	Product size (bp)
B2m-F	TACGCCTGCAGAGTTAAGCA	71
B2m-R	GATCACATGTCTCGATCCCAGT	
*Hprt*1-F	GGGGGACATAAAAGTTATTGGTGG	70
*Hprt*1-R	TTCAACAATCAAGACATTCTTTCCA	
Ankh-F	TCACCACATAGCCATCGAC	73
Ankh-R	ACTGCATCCTCCTGACTGC	
Ankh-2F2	CTGCTGCTACAGAGGCAGTG	215
Ankh-2R2	GACAAAACAGAGCGTCAGCGA	
Ankh-2F3	AACTGGCGAACACAAGCAAC	92

Ankh-2R3	GACAAAACAGAGCGTCAGCG	

Statistical methods

Human and mouse data where the numbers of repeats were the same were analysed by the Student's unpaired test. Where the repeat numbers were uneven human data were analysed by the Welch's T test and the mouse data was analysed using the Mann-Whitney Test, the significance level was set at $p < 0.05$.

References.

1. Campisi J, Kapahi P, Lithgow GJ, Melov S, Newman JC, Verdin E. From discoveries in ageing research to therapeutics for healthy ageing. Nature. 2019;571(7764):183-92.
2. Mattison JA, Colman RJ, Beasley TM, Allison DB, Kemnitz JW, Roth GS, et al. Caloric restriction improves health and survival of rhesus monkeys. Nat Commun. 2017;8:14063.
3. Fontana L, Mitchell SE, Wang B, Tosti V, van Vliet T, Veronese N, et al. The effects of graded caloric restriction: XII. Comparison of mouse to human impact on cellular senescence in the colon. Aging Cell. 2018;17(3):e12746.
4. Krishnamurthy J, Torrice C, Ramsey MR, Kovalev GI, Al-Regaiey K, Su L, et al. Ink4a/Arf expression is a biomarker of aging. J Clin Invest. 2004;114(9):1299-307.
5. Lin HT, Cheng ML, Lo CJ, Hsu WC, Lin G, Liu FC. (1)H NMR metabolomic profiling of human cerebrospinal fluid in aging process. Am J Transl Res. 2021;13(11):12495-508.
6. Mycielska ME, James EN, Parkinson EK. Metabolic Alterations in Cellular Senescence: The Role of Citrate in Ageing and Age-Related Disease. Int J Mol Sci. 2022;23(7).
7. Varshavi D, Scott FH, Varshavi D, Veeravalli S, Phillips IR, Veselkov K, et al. Metabolic Biomarkers of Ageing in C57BL/6J Wild-Type and Flavin-Containing Monooxygenase 5 (FMO5)-Knockout Mice. Front Mol Biosci. 2018;5:28.
8. Yue T, Tan H, Shi Y, Xu M, Luo S, Weng J, et al. Serum Metabolomic Profiling in Aging Mice Using Liquid Chromatography-Mass Spectrometry. Biomolecules. 2022;12(11).
9. Birkenfeld AL, Lee HY, Guebre-Egziabher F, Alves TC, Jurczak MJ, Jornayvaz FR, et al. Deletion of the mammalian INDY homolog mimics aspects of dietary restriction and protects against adiposity and insulin resistance in mice. Cell Metab. 2011;14(2):184-95.
10. Branco JR, Esteves AM, Imbroisi Filho R, Demaria TM, Lisboa PC, Lopes BP, et al. Citrate enrichment in a Western diet reduces weight gain via browning of adipose tissues without resolving diet-induced insulin resistance in mice. Food Funct. 2022;13(21):10947-55.
11. Fan SZ, Lin CS, Wei YW, Yeh SR, Tsai YH, Lee AC, et al. Dietary citrate supplementation enhances longevity, metabolic health, and memory performance through promoting ketogenesis. Aging Cell. 2021;20(12):e13510.
12. Fan SZ, Sung CW, Tsai YH, Yeh SR, Lin WS, Wang PY. Nervous System Deletion of Mammalian INDY in Mice Mimics Dietary Restriction-Induced Memory Enhancement. J Gerontol A Biol Sci Med Sci. 2021;76(1):50-6.
13. Willmes DM, Daniels M, Kurzbach A, Lieske S, Bechmann N, Schumann T, et al. The longevity gene mIndy (I'm Not Dead, Yet) affects blood pressure through sympathoadrenal mechanisms. JCI Insight. 2021;6(2).
14. Zahn G, Willmes DM, El-Agroudy NN, Yarnold C, Jarjes-Pike R, Schaertl S, et al. A Novel and Cross-Species Active Mammalian INDY (NaCT) Inhibitor Ameliorates Hepatic Steatosis in Mice with Diet-Induced Obesity. Metabolites. 2022;12(8).
15. Drexler K, Schmidt KM, Jordan K, Federlin M, Milenkovic VM, Liebisch G, et al. Cancer-associated cells release citrate to support tumour metastatic progression. Life Sci Alliance. 2021;4(6).
16. Mycielska ME, Dettmer K, Rummele P, Schmidt K, Prehn C, Milenkovic VM, et al. Extracellular Citrate Affects Critical Elements of Cancer Cell Metabolism and Supports Cancer Development In Vivo. Cancer Res. 2018;78(10):2513-23.
17. Fernandez-Fuente G, Overmyer KA, Lawton AJ, Kasza I, Shapiro SL, Gallego-Munoz P, et al. The citrate transporters SLC13A5 and SLC25A1 elicit different metabolic responses and phenotypes in the mouse. Commun Biol. 2023;6(1):926.
18. Anerillas C, Mazan-Mamczarz K, Herman AB, Munk R, Lam KG, Calvo-Rubio M, et al. The YAP-TEAD complex promotes senescent cell survival by lowering endoplasmic reticulum stress. Nat Aging. 2023;3(10):1237-50.

19. Jaramillo-Martinez V, Sivaprakasam S, Ganapathy V, Urbatsch IL. Drosophila INDY and Mammalian INDY: Major Differences in Transport Mechanism and Structural Features despite Mostly Similar Biological Functions. Metabolites. 2021;11(10).
20. Zahn G, Baukmann HA, Wu J, Jordan J, Birkenfeld AL, Dirckx N, et al. Targeting Longevity Gene SLC13A5: A Novel Approach to Prevent Age-Related Bone Fragility and Osteoporosis. Metabolites. 2023;13(12).
21. Dirckx N, Zhang Q, Chu EY, Tower RJ, Li Z, Guo S, et al. A specialized metabolic pathway partitions citrate in hydroxyapatite to impact mineralization of bones and teeth. Proc Natl Acad Sci U S A. 2022;119(45):e2212178119.
22. Gill D, Zagkos L, Gill R, Benzing T, Jordan J, Birkenfeld AL, et al. The citrate transporter SLC13A5 as a therapeutic target for kidney disease: evidence from Mendelian randomization to inform drug development. BMC Med. 2023;21(1):504.
23. James EL, Michalek RD, Pitiyage GN, de Castro AM, Vignola KS, Jones J, et al. Senescent human fibroblasts show increased glycolysis and redox homeostasis with extracellular metabolomes that overlap with those of irreparable DNA damage, aging, and disease. J Proteome Res. 2015;14(4):1854-71.
24. James ENL, Bennett MH, Parkinson EK. The induction of the fibroblast extracellular senescence metabolome is a dynamic process. Sci Rep. 2018;8(1):12148.
25. James EN, Sagi-Kiss V, Bennett M, Mycielska ME, Karen-Ng LP, Roberts T, et al. Dyskeratosis Congenita links telomere attrition to age-related systemic energetics. J Gerontol A Biol Sci Med Sci. 2023.
26. Park YJ, Kim JC, Kim Y, Kim YH, Park SS, Muther C, et al. Senescent melanocytes driven by glycolytic changes are characterized by melanosome transport dysfunction. Theranostics. 2023;13(12):3914-24.
27. Delfarah A, Parrish S, Junge JA, Yang J, Seo F, Li S, et al. Inhibition of nucleotide synthesis promotes replicative senescence of human mammary epithelial cells. J Biol Chem. 2019;294(27):10564-78.
28. Jenkins CM, Yang J, Sims HF, Gross RW. Reversible high affinity inhibition of phosphofructokinase-1 by acyl-CoA: a mechanism integrating glycolytic flux with lipid metabolism. J Biol Chem. 2011;286(14):11937-50.
29. Ma Z, Ding Y, Ding X, Mou H, Mo R, Tan Q. PDK4 rescues high-glucose-induced senescent fibroblasts and promotes diabetic wound healing through enhancing glycolysis and regulating YAP and JNK pathway. Cell Death Discov. 2023;9(1):424.
30. Szeri F, Lundkvist S, Donnelly S, Engelke UFH, Rhee K, Williams CJ, et al. The membrane protein ANKH is crucial for bone mechanical performance by mediating cellular export of citrate and ATP. PLoS Genet. 2020;16(7):e1008884.
31. Ho AM, Johnson MD, Kingsley DM. Role of the mouse ank gene in control of tissue calcification and arthritis. Science. 2000;289(5477):265-70.
32. Shin SY, Fauman EB, Petersen AK, Krumsiek J, Santos R, Huang J, et al. An atlas of genetic influences on human blood metabolites. Nat Genet. 2014;46(6):543-50.
33. Bellenguez C, Kucukali F, Jansen IE, Kleineidam L, Moreno-Grau S, Amin N, et al. New insights into the genetic etiology of Alzheimer's disease and related dementias. Nat Genet. 2022;54(4):412-36.
34. Stewart SA, Hahn WC, O'Connor BF, Banner EN, Lundberg AS, Modha P, et al. Telomerase contributes to tumorigenesis by a telomere length-independent mechanism. Proc Natl Acad Sci U S A. 2002;99(20):12606-11.
35. Hahn WC, Stewart SA, Brooks MW, York SG, Eaton E, Kurachi A, et al. Inhibition of telomerase limits the growth of human cancer cells. Nat Med. 1999;5(10):1164-70.
36. Counter CM, Hahn WC, Wei W, Caddle SD, Beijersbergen RL, Lansdorp PM, et al. Dissociation among in vitro telomerase activity, telomere maintenance, and cellular immortalization. Proc Natl Acad Sci U S A. 1998;95(25):14723-8.

37. Freund A, Patil CK, Campisi J. p38MAPK is a novel DNA damage response-independent regulator of the senescence-associated secretory phenotype. EMBO J. 2011;30(8):1536-48.
38. Laberge RM, Sun Y, Orjalo AV, Patil CK, Freund A, Zhou L, et al. MTOR regulates the pro-tumorigenic senescence-associated secretory phenotype by promoting IL1A translation. Nat Cell Biol. 2015;17(8):1049-61.
39. Rodier F, Coppe JP, Patil CK, Hoeijmakers WA, Munoz DP, Raza SR, et al. Persistent DNA damage signalling triggers senescence-associated inflammatory cytokine secretion. Nat Cell Biol. 2009;11(8):973-9.
40. Alimbetov D, Davis T, Brook AJ, Cox LS, Faragher RG, Nurgozhin T, et al. Suppression of the senescence-associated secretory phenotype (SASP) in human fibroblasts using small molecule inhibitors of p38 MAP kinase and MK2. Biogerontology. 2016;17(2):305-15.
41. Iwasa H, Han J, Ishikawa F. Mitogen-activated protein kinase p38 defines the common senescence-signalling pathway. Genes Cells. 2003;8(2):131-44.
42. Laberge RM, Zhou L, Sarantos MR, Rodier F, Freund A, de Keizer PL, et al. Glucocorticoids suppress selected components of the senescence-associated secretory phenotype. Aging Cell. 2012;11(4):569-78.
43. Justice JN, Nambiar AM, Tchkonia T, LeBrasseur NK, Pascual R, Hashmi SK, et al. Senolytics in idiopathic pulmonary fibrosis: Results from a first-in-human, open-label, pilot study. EBioMedicine. 2019;40:554-63.
44. Stowe RP, Peek MK, Cutchin MP, Goodwin JS. Plasma cytokine levels in a population-based study: relation to age and ethnicity. J Gerontol A Biol Sci Med Sci. 2010;65(4):429-33.
45. Pazolli E, Alspach E, Milczarek A, Prior J, Piwnica-Worms D, Stewart SA. Chromatin remodeling underlies the senescence-associated secretory phenotype of tumor stromal fibroblasts that supports cancer progression. Cancer Res. 2012;72(9):2251-61.
46. Sablina AA, Budanov AV, Ilyinskaya GV, Agapova LS, Kravchenko JE, Chumakov PM. The antioxidant function of the p53 tumor suppressor. Nat Med. 2005;11(12):1306-13.
47. Shipley GD, Pittelkow MR, Wille JJ, Jr., Scott RE, Moses HL. Reversible inhibition of normal human prokeratinocyte proliferation by type beta transforming growth factor-growth inhibitor in serum-free medium. Cancer Res. 1986;46(4 Pt 2):2068-71.
48. Acosta JC, Banito A, Wuestefeld T, Georgilis A, Janich P, Morton JP, et al. A complex secretory program orchestrated by the inflammasome controls paracrine senescence. Nat Cell Biol. 2013;15(8):978-90.
49. Hassona Y, Cirillo N, Lim KP, Herman A, Mellone M, Thomas GJ, et al. Progression of genotype-specific oral cancer leads to senescence of cancer-associated fibroblasts and is mediated by oxidative stress and TGF-beta. Carcinogenesis. 2013;34(6):1286-95.
50. Chapman S, Liu X, Meyers C, Schlegel R, McBride AA. Human keratinocytes are efficiently immortalized by a Rho kinase inhibitor. J Clin Invest. 2010;120(7):2619-26.
51. Harle-Bachor C, Boukamp P. Telomerase activity in the regenerative basal layer of the epidermis inhuman skin and in immortal and carcinoma-derived skin keratinocytes. Proc Natl Acad Sci U S A. 1996;93(13):6476-81.
52. Loughran O, Malliri A, Owens D, Gallimore PH, Stanley MA, Ozanne B, et al. Association of CDKN2A/p16INK4A with human head and neck keratinocyte replicative senescence: relationship of dysfunction to immortality and neoplasia. Oncogene. 1996;13(3):561-8.
53. Ogrodnik M, Evans SA, Fielder E, Victorelli S, Kruger P, Salmonowicz H, et al. Whole-body senescent cell clearance alleviates age-related brain inflammation and cognitive impairment in mice. Aging Cell. 2021;20(2):e13296.
54. Xu M, Pirtskhalava T, Farr JN, Weigand BM, Palmer AK, Weivoda MM, et al. Senolytics improve physical function and increase lifespan in old age. Nat Med. 2018;24(8):1246-56.

55. Palmer AK, Xu M, Zhu Y, Pirtskhalava T, Weivoda MM, Hachfeld CM, et al. Targeting senescent cells alleviates obesity-induced metabolic dysfunction. Aging Cell. 2019:e12950.
56. Zhang X, Habiballa L, Aversa Z, Ng YE, Sakamoto AE, Englund DA, et al. Characterization of cellular senescence in aging skeletal muscle. Nat Aging. 2022;2(7):601-15.
57. Marthandan S, Priebe S, Hemmerich P, Klement K, Diekmann S. Long-term quiescent fibroblast cells transit into senescence. PLoS One. 2014;9(12):e115597.
58. Munro J, Steeghs K, Morrison V, Ireland H, Parkinson EK. Human fibroblast replicative senescence can occur in the absence of extensive cell division and short telomeres. Oncogene. 2001;20(27):3541-52.
59. Wootton M, Steeghs K, Watt D, Munro J, Gordon K, Ireland H, et al. Telomerase alone extends the replicative life span of human skeletal muscle cells without compromising genomic stability. Hum Gene Ther. 2003;14(15):1473-87.
60. Mycielska ME, Milenkovic VM, Wetzel CH, Rummele P, Geissler EK. Extracellular Citrate in Health and Disease. Curr Mol Med. 2015;15(10):884-91.
61. Rapisarda V, Borghesan M, Miguela V, Encheva V, Snijders AP, Lujambio A, et al. Integrin Beta 3 Regulates Cellular Senescence by Activating the TGF-beta Pathway. Cell Rep. 2017;18(10):2480-93.
62. Bhat R, Crowe EP, Bitto A, Moh M, Katsetos CD, Garcia FU, et al. Astrocyte senescence as a component of Alzheimer's disease. PLoS One. 2012;7(9):e45069.
63. Herranz N, Gallage S, Mellone M, Wuestefeld T, Klotz S, Hanley CJ, et al. mTOR regulates MAPKAPK2 translation to control the senescence-associated secretory phenotype. Nat Cell Biol. 2015;17(9):1205-17.
64. Ozcan L, Xu X, Deng SX, Ghorpade DS, Thomas T, Cremers S, et al. Treatment of Obese Insulin-Resistant Mice With an Allosteric MAPKAPK2/3 Inhibitor Lowers Blood Glucose and Improves Insulin Sensitivity. Diabetes. 2015;64(10):3396-405.
65. Jurk D, Wilson C, Passos JF, Oakley F, Correia-Melo C, Greaves L, et al. Chronic inflammation induces telomere dysfunction and accelerates ageing in mice. Nat Commun. 2014;2:4172.
66. Gopal E, Babu E, Ramachandran S, Bhutia YD, Prasad PD, Ganapathy V. Species-specific influence of lithium on the activity of SLC13A5 (NaCT): lithium-induced activation is specific for the transporter in primates. J Pharmacol Exp Ther. 2015;353(1):17-26.
67. Jeon OH, Mehdipour M, Gil TH, Kang M, Aguirre NW, Robinson ZR, et al. Systemic induction of senescence in young mice after single heterochronic blood exchange. Nat Metab. 2022;4(8):995-1006.
68. Bussian TJ, Aziz A, Meyer CF, Swenson BL, van Deursen JM, Baker DJ. Clearance of senescent glial cells prevents tau-dependent pathology and cognitive decline. Nature. 2018;562(7728):578-82.
69. Tesi N, van der Lee S, Hulsman M, van Schoor NM, Huisman M, Pijnenburg Y, et al. Cognitively healthy centenarians are genetically protected against Alzheimer's disease. Alzheimers Dement. 2024;20(6):3864-75.
70. Bhutia YD, Kopel JJ, Lawrence JJ, Neugebauer V, Ganapathy V. Plasma Membrane Na(+)-Coupled Citrate Transporter (SLC13A5) and Neonatal Epileptic Encephalopathy. Molecules. 2017;22(3).
71. Ashbrook MJ, McDonough KL, Pituch JJ, Christopherson PL, Cornell TT, Selewski DT, et al. Citrate modulates lipopolysaccharide-induced monocyte inflammatory responses. Clin Exp Immunol. 2015;180(3):520-30.
72. Leandro JG, Espindola-Netto JM, Vianna MC, Gomez LS, DeMaria TM, Marinho-Carvalho MM, et al. Exogenous citrate impairs glucose tolerance and promotes visceral adipose tissue inflammation in mice. Br J Nutr. 2016;115(6):967-73.

73. von Loeffelholz C, Lieske S, Neuschafer-Rube F, Willmes DM, Raschzok N, Sauer IM, et al. The human longevity gene homolog INDY and interleukin-6 interact in hepatic lipid metabolism. Hepatology. 2017;66(2):616-30.
74. Baker DJ, Childs BG, Durik M, Wijers ME, Sieben CJ, Zhong J, et al. Naturally occurring p16(Ink4a)-positive cells shorten healthy lifespan. Nature. 2016;530(7589):184-9.
75. Huard K, Brown J, Jones JC, Cabral S, Futatsugi K, Gorgoglione M, et al. Discovery and characterization of novel inhibitors of the sodium-coupled citrate transporter (NaCT or SLC13A5). Sci Rep. 2015;5:17391.
76. Dow CT, Harley CB. Evaluation of an oral telomerase activator for early age-related macular degeneration - a pilot study. Clin Ophthalmol. 2016;10:243-9.
77. Eitan E, Tichon A, Gazit A, Gitler D, Slavin S, Priel E. Novel telomerase-increasing compound in mouse brain delays the onset of amyotrophic lateral sclerosis. EMBO Mol Med. 2012;4(4):313-29.
78. Shim HS, Iaconelli J, Shang X, Li J, Lan ZD, Jiang S, et al. TERT activation targets DNA methylation and multiple aging hallmarks. Cell. 2024;187(15):4030-42 e13.
79. Munro J, Stott FJ, Vousden KH, Peters G, Parkinson EK. Role of the alternative INK4A proteins in human keratinocyte senescence: evidence for the specific inactivation of p16INK4A upon immortalization. Cancer Res. 1999;59(11):2516-21.
80. Karen-Ng LP, Ahmad US, Gomes L, Hunter KD, Wan H, Hagi-Pavli E, et al. Extracellular Prostaglandins E1 and E2 and Inflammatory Cytokines Are Regulated by the Senescence Program in Potentially Premalignant Oral Keratinocytes. Cancers (Basel). 2022;14(11).
81. Dickson MA, Hahn WC, Ino Y, Ronfard V, Wu JY, Weinberg RA, et al. Human keratinocytes that express hTERT and also bypass a p16(INK4a)-enforced mechanism that limits life span become immortal yet retain normal growth and differentiation characteristics. Mol Cell Biol. 2000;20(4):1436-47.
82. Mazurek MP, Prasad PD, Gopal E, Fraser SP, Bolt L, Rizaner N, et al. Molecular origin of plasma membrane citrate transporter in human prostate epithelial cells. EMBO Rep. 2010;11(6):431-7.
83. Swift S, Lorens J, Achacoso P, Nolan GP. Rapid production of retroviruses for efficient gene delivery to mammalian cells using 293T cell-based systems. Curr Protoc Immunol. 2001;Chapter 10:Unit 10 7C.
84. Morgan JR, Barrandon Y, Green H, Mulligan RC. Expression of an exogenous growth hormone gene by transplantable human epidermal cells. Science. 1987;237(4821):1476-9.
85. Wege H, Chui MS, Le HT, Tran JM, Zern MA. SYBR Green real-time telomeric repeat amplification protocol for the rapid quantification of telomerase activity. Nucleic Acids Res. 2003;31(2):E3-.
86. Kim NW, Wu F. Advances in quantification and characterization of telomerase activity by the telomeric repeat amplification protocol (TRAP). Nucleic Acids Res. 1997;25(13):2595-7.
87. Ducrest AL, Amacker M, Mathieu YD, Cuthbert AP, Trott DA, Newbold RF, et al. Regulation of human telomerase activity: repression by normal chromosome 3 abolishes nuclear telomerase reverse transcriptase transcripts but does not affect c-Myc activity. Cancer Res. 2001;61(20):7594-602.
88. Smith KM, Wilson ID, Rainville PD. Sensitive and Reproducible Mass Spectrometry-Compatible RP-UHPLC Analysis of Tricarboxylic Acid Cycle and Related Metabolites in Biological Fluids: Application to Human Urine. Anal Chem. 2021;93(2):1009-15.
89. Teh MT, Hutchison IL, Costea DE, Neppelberg E, Liavaag PG, Purdie K, et al. Exploiting FOXM1-orchestrated molecular network for early squamous cell carcinoma diagnosis and prognosis. Int J Cancer. 2013;132(9):2095-106.
90. Gemenetzidis E, Bose A, Riaz AM, Chaplin T, Young BD, Ali M, et al. FOXM1 upregulation is an early event in human squamous cell carcinoma and it is enhanced by nicotine during malignant transformation. PLoS One. 2009;4(3):e4849.

91. Teh MT, Gemenetzidis E, Chaplin T, Young BD, Philpott MP. Upregulation of FOXM1 induces genomic instability in human epidermal keratinocytes. Mol Cancer. 2010;9(1):45.
92. Waseem A, Ali M, Odell EW, Fortune F, Teh MT. Downstream targets of FOXM1: CEP55 and HELLS are cancer progression markers of head and neck squamous cell carcinoma. Oral Oncol. 2010;46(7):536-42.
93. Bustin SA, Benes V, Garson JA, Hellemans J, Huggett J, Kubista M, et al. The MIQE guidelines: minimum information for publication of quantitative real-time PCR experiments. Clin Chem. 2009;55(4):611-22.
94. Zhao S, Fernald RD. Comprehensive algorithm for quantitative real-time polymerase chain reaction. J Comput Biol. 2005;12(8):1047-64.
95. Vandesompele J, De Preter K, Pattyn F, Poppe B, Van Roy N, De Paepe A, et al. Accurate normalization of real-time quantitative RT-PCR data by geometric averaging of multiple internal control genes. Genome Biol. 2002;3(7):RESEARCH0034.

Author Contributions

Emma Naomi James and Mark Bennett performed the gas chromatography/mass spectroscopy analysis; Yufeng Li and Jacob Bundy performed the liquid chromatography/ mass spectroscopy analysis; Muy Teck The performed the multiplex quantitative PCR analysis; Zahra Falah Hassan Al-Khateeb and Adina Michael-Titus provided the mouse brain RNA and senescence data; Ana O'Loghlen provided the previously characterised mouse liver and kidney RNA samples; Christine Wagner performed the western blots for metabolite transporters in human cell extracts[1], Lee Peng Karen-Ng and Linnea Synchyshyn performed the cytokine analysis; Terry Roberts performed the TERT qPCR and telomerase activity assays , Amy Lewis and Andrew Silver performed the In Cell analysis of the sodium butyrate experiments; Eric Kenneth Parkinson performed al the human in vitro work and wrote the first draft of the manuscript; Maria Mycielska and Eric Kenneth Parkinson conceived the study and wrote the first draft of the manuscript.

Acknowledgements

The authors wish to thank Cleo Bishop and Emily Anne O'Sullivan for advice regarding knockdown using Horizon Discovery shRNAs, Gary Warnes for performing the cell sorting and Simon McArthur for advice on markers of brain ageing. We also wish to thank John Sedivy of Brown University, Rhode Island for the gift of the Loxo26 cell lines.

Funding

The study was funded in part by the Dunhill Medical Trust (grant number R452/1115) and Barts and the London Charity (grant number MRD&U0004). Karen-Ng Lee Peng received a Ph.D. scholarship (Hadiah Latihan Persekutuan) from the Malaysian Ministry of Education. Ana O'Loghlen received funding from Barts Charity Grants (G-002158) and Project I+D+i PID2021-125656OB-I00, financed by MCIN/ AEI /10.13039/501100011033/FEDER, UE and Project SenesceX-CM P2022/BMD-7393.

Conflict of interest statement

Maria Mycielska is a co-inventor on the Patent Application no. EP15767532.3 and US2020/408741 (status patent pending) and US2017/0241981 (patent issued) “The plasma membrane citrate transporter for use in the diagnosis and treatment of cancer” owned by the University Hospital Regensburg. The other authors declare no conflict of interest.

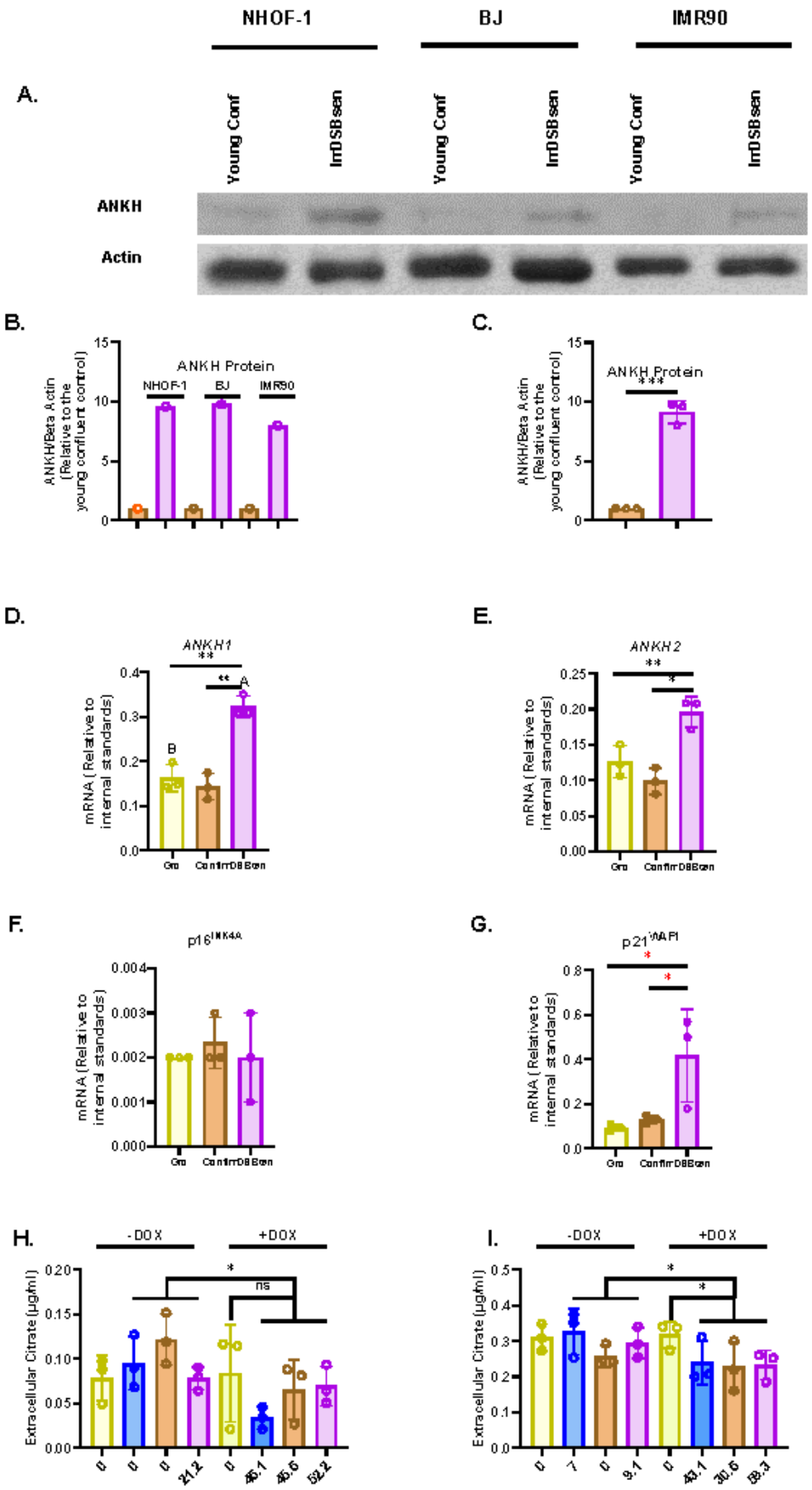
NHOF-1
BJ
IMR90
A.
Young Conf
ImDSBsen
ANKH
Actin
B.
ANKH Protein
ANKH/Beta Actin (Relative to the young confluent control)
C.
D.
ANKH1
mRNA (Relative to internal standards)
E.
ANKH2
F.
p16INK4A
G.
p21WAF1
H.
-DOX
+DOX
Extracellular Citrate (µg/ml)
I.

Figure 1 *ANKH* protein and transcript are upregulated in IrrDSBsen human fibroblasts.

A. Shows a western blot of *ANKH* protein in 3 lines of quiescent confluent (Conf) young human fibroblasts and the same lines induced to senesce by ionising radiation (IrrDSBsen). Beta actin was used as a loading control.

B. Image J quantitation of the blot in A. showing the levels of *ANKH* signal versus beta actin in all conditions after background subtraction.

C. The average of the values in B.

D. The expression of *ANKH* mRNA in growing confluent and IrrDSBsen NHOF-1 cells using primer set 1.

E . As in D. but the results of primer set 2 in the same experiments.

F. As in D. but the expression of the senescence marker $p16^{INK4A}$in the same experiments.

G. As in D. but the expression of the senescence marker $p21^{WAF1}$ in the same experiments.

B-G. Yellow bars = growing cells; light brown bars = confluent cells; purple bars = IrrDSBsen cells.

H. The effect of inducible *ANKH* shRNA vectors and their non-targeting (NT) controls with and without the doxycyclin inducer (DOX) on growing NHOF-1 cells. The numbers below each bar represent the level of *ANKH* mRNA knockdown. Yellow bars = NT control; blue bars = shRNA #1002; dark brown bars = shRNA #2500; purple bars = shRNA #5474.

I. The effect of inducible *ANKH* shRNA vectors and their non-targeting (NT) controls with and without the doxycyclin inducer (DOX) on IrrDSBsen NHOF-1 cells. The numbers below each bar represent the level of *ANKH* mRNA knockdown. The symbols are the same as for H.

In all experiments * = P< 0.05; ** = P < 0.01; *** = P < 0.001; * trend for significance; ns = not significant. The results are averages +/- standard deviation. N = 3.

The experiments in A.- C, D.- G and H-I. were performed at different times but using identical cell culture protocols and reagents.

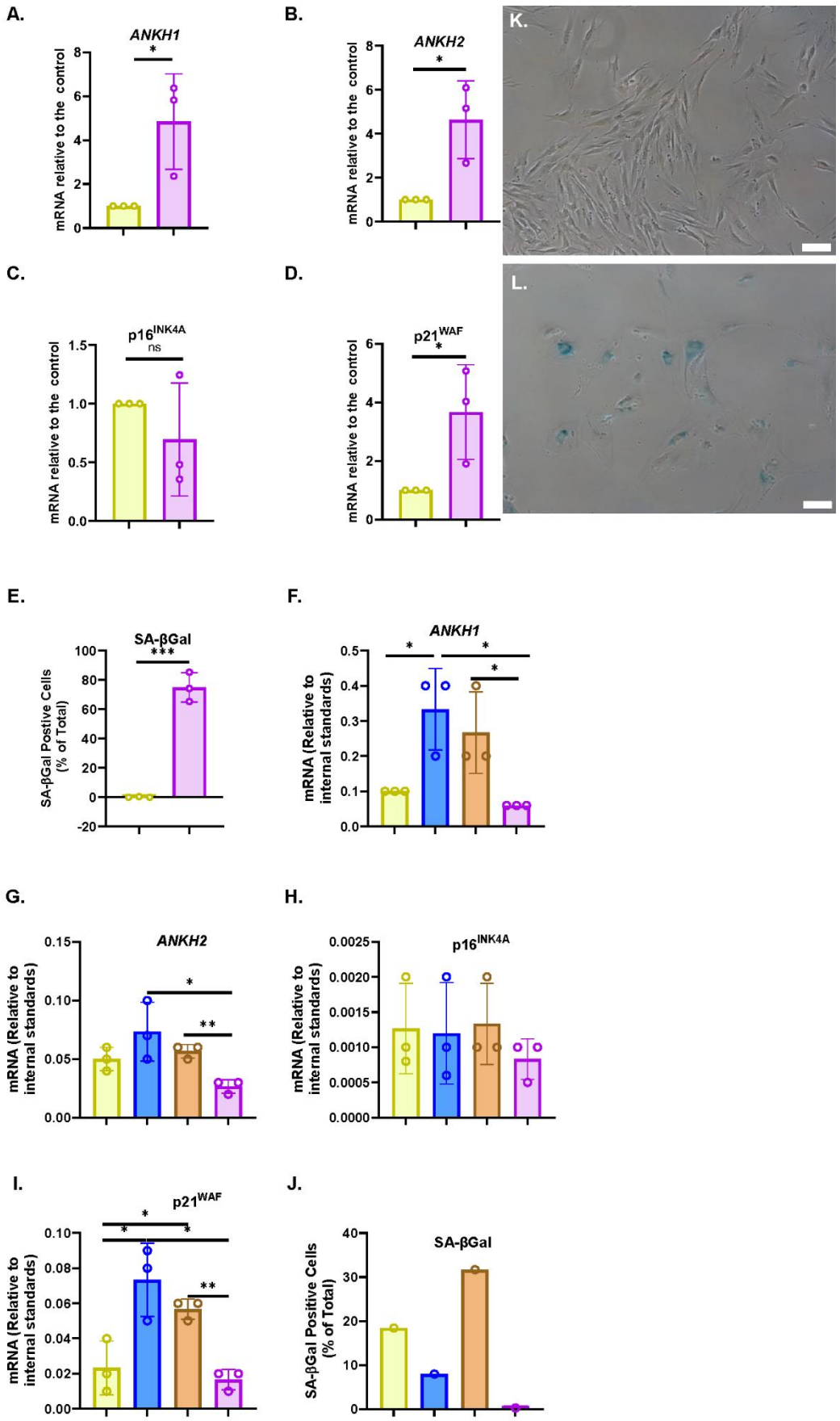
A.
ANKH1
mRNA relative to the control
B.
ANKH2
mRNA relative to the control
K.
C.
p16INK4A
ns
mRNA relative to the control
D.
p21WAF
mRNA relative to the control
L.
E.
SA-βGal
SA-βGal Postive Cells (% of Total)
F.
ANKH1
mRNA (Relative to internal standards)
G.
ANKH2
mRNA (Relative to internal standards)
H.
p16INK4A
mRNA (Relative to internal standards)
I.
p21WAF
mRNA (Relative to internal standards)
J.
SA-βGal
SA-βGal Positive Cells (% of Total)

Figure 2 *ANKH* transcript is upregulated in PEsen human fibroblasts and downregulated by telomerase.

A. The expression of *ANKH* mRNA in growing and PEsen NHOF-1 cells using primer set 1.

B . As in A. but the results of primer set 2 in the same experiments.

C. As in A. but the expression of the senescence marker $p16^{INK4A}$in the same experiments.

D. As in A. but the expression of the senescence marker $p21^{WAF1}$ in the same experiments.

E. As in A. but showing SA-β Gal expression.

A-E. White bars = growing young cells 20.2-21 MPDs; light grey bars = PEsen cells 68.2 MPDs. * = P< 0.05; ** = P < 0.01; *** = P < 0.001; * trend for significance; ns = not significant. The results are averages +/- standard deviation. N = 3.

F. The expression of *ANKH* mRNA in NHOF-1 PURO, TERT-HA, DN TERT and TERT cell using primer set 1. N =3.

G. As in F. but the results of primer set 2 in the same experiments.

H. As in F. but the expression of the senescence marker $p16^{INK4A}$in the same experiments.

I. As in F. but the expression of the senescence marker $p21^{WAF1}$ in the same experiments.

J. As in F. but showing SA-β Gal expression.

K. and L. Representative images of SA-βGal staining in E; K. Young growing NHOF-1 fibroblasts (20.2 MPDs), L. NHOF-1 cells (68.2 MPDs). Bar = 100µm

F-J. A-E. Yellow bars = LATE PURO; blue bars TERT-HA, brown bars DN TERT and purple bars TERT all after completing 60 MPDs. * = P< 0.05; ** = P < 0.01; *** = P < 0.001; * trend for significance; ns = not significant. The results are averages +/- standard deviation. N = 4, except J.

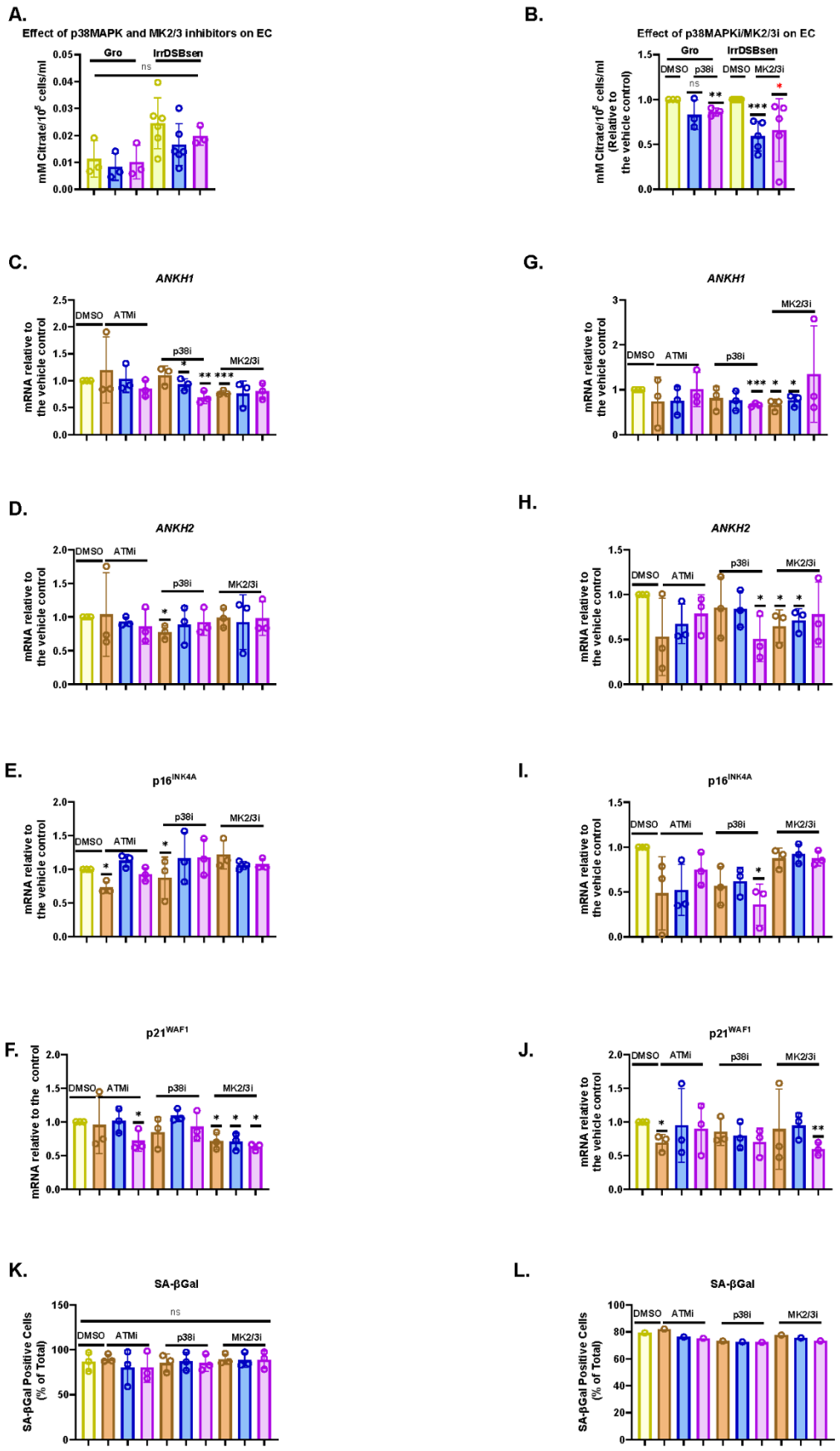
A.
Effect of p38MAPK and MK2/3 inhibitors on EC
mM Citrate/10^5 cells/ml
Gro
IrrDSBsen
ns
B.
Effect of p38MAPKi/MK2/3i on EC
mM Citrate/10^5 cells/ml (Relative to the vehicle control)
DMSO
p38i
MK2/3i
C.
ANKH1
mRNA relative to the vehicle control
DMSO
ATMi
p38i
MK2/3i
D.
ANKH2
E.
p16INK4A
F.
p21WAF1
mRNA relative to the control
G.
H.
I.
J.
K.
SA-βGal
SA-βGal Positive Cells (% of Total)
L.

Figure 3 The p38 mitogen-activated kinase, the (*p38MAPK*)/MAPK-activated kinase2/3 (*MAPKAPK 2/3*) and the Ataxia Telangiectasia Mutated (*ATM*) kinase regulate EC, secreted IL-6 and *ANKH* mRNA expression differently in human fibroblasts.

A, The effect of SB203580 (p38 inhibitor) and PF-3644022 (MK2/3 inhibitor) on EC in young growing and IrrDSBsen NHOF-1 cells (N =3). Yellow bars DMSO (vehicle) control; blue bars = SB203580 10 µM;; purple bars = PF-3644022 2.5 µM

B. The same data as in A and a separate series of experiments but normalised to the DMSO vehicle control (N = 6).

C-K. The effect of the kinase inhibitors SB203580 (p38MAPK) the PF-3644022 (MK2/3) and KU55933 (ATM) on *ANKH* transcript and senescence markers in IrrDSBsen cells. C-F BJ cells; G-J NHOF-1 cells.

C. and G. The expression of *ANKH* mRNA using primer set 1.

D. and H. The expression of *ANKH* mRNA using primer set 2.

E. and I. The expression of $p16^{INK4A}$ mRNA.

F. and J. The expression of $p21^{WAF1}$ mRNA.

K. and L. SA-β Gal expression (%).

Yellow bars DMSO (vehicle) control; brown bars 1 µM; blue bars 3 µM; purple bars 10 µm * = P< 0.05; ** = P < 0.01; *** = P < 0.001; * trend for significance; ns = not significant. The results are averages +/- standard deviation (N =3 except in B. where N =6).

The experiments in A.- B. and C.- L. were performed at different times but using identical cell culture protocols and reagents.

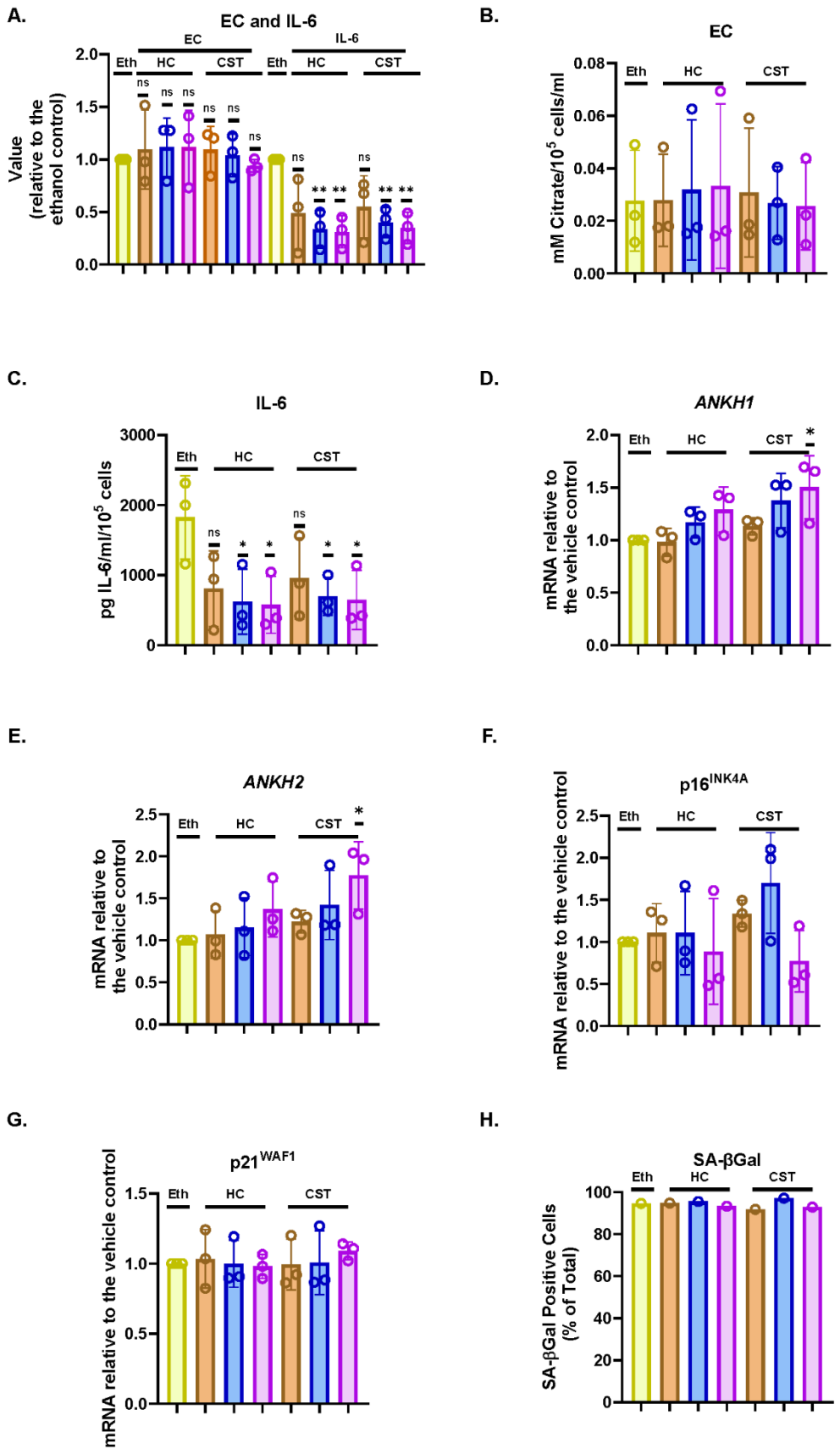
A.
EC and IL-6
EC
IL-6
Eth
HC
CST
Value (relative to the ethanol control)
ns
**
B.
EC
mM Citrate/10^5 cells/ml
C.
IL-6
pg IL-6/ml/10^5 cells
*
D.
ANKH1
mRNA relative to the vehicle control
E.
ANKH2
F.
p16^INK4A
G.
p21^WAF1
H.
SA-βGal
SA-βGal Positive Cells (% of Total)

Figure 4. The effect of steroids on the EC, *ANKH* expression and secreted IL-6 in IrrDSBsen human fibroblasts

A. Shows the EC and IL-6 levels in the medium of IrrDSBsen BJ fibroblasts after treatment with the indicated doses of HC and CST.

B. Shows the absolute EC levels in mM citrate per 10^5 cells per ml from the experiment in A.

C. Shows the absolute levels of IL-6 in pg/ml per 10^5 cells from the experiment in A.

D. The effect the indicated doses of HC and CST on the expression of *ANKH* mRNA using primer set 1.

E. As in D. but the results of primer set 2 in the same experiments.

F. As in D. but the expression of the senescence marker $p16^{INK4A}$in the same experiments.

G. As in D. but the expression of the senescence marker $p21^{WAF1}$ in the same experiments.

H. As in D. but the expression of senescence marker SA-βGal in the same experiments.

Yellow bars control; brown bars 30nM; blue bars 100nM; purple bars 300nM * = P< 0.05; ** = P < 0.01; *** = P < 0.001; ns = not significant. The results are averages +/- standard deviation. A. to G. N = 3. H. N=1.

The experiments in A.- C. and D.- L. were performed at separate times but using identical protocols and reagents.

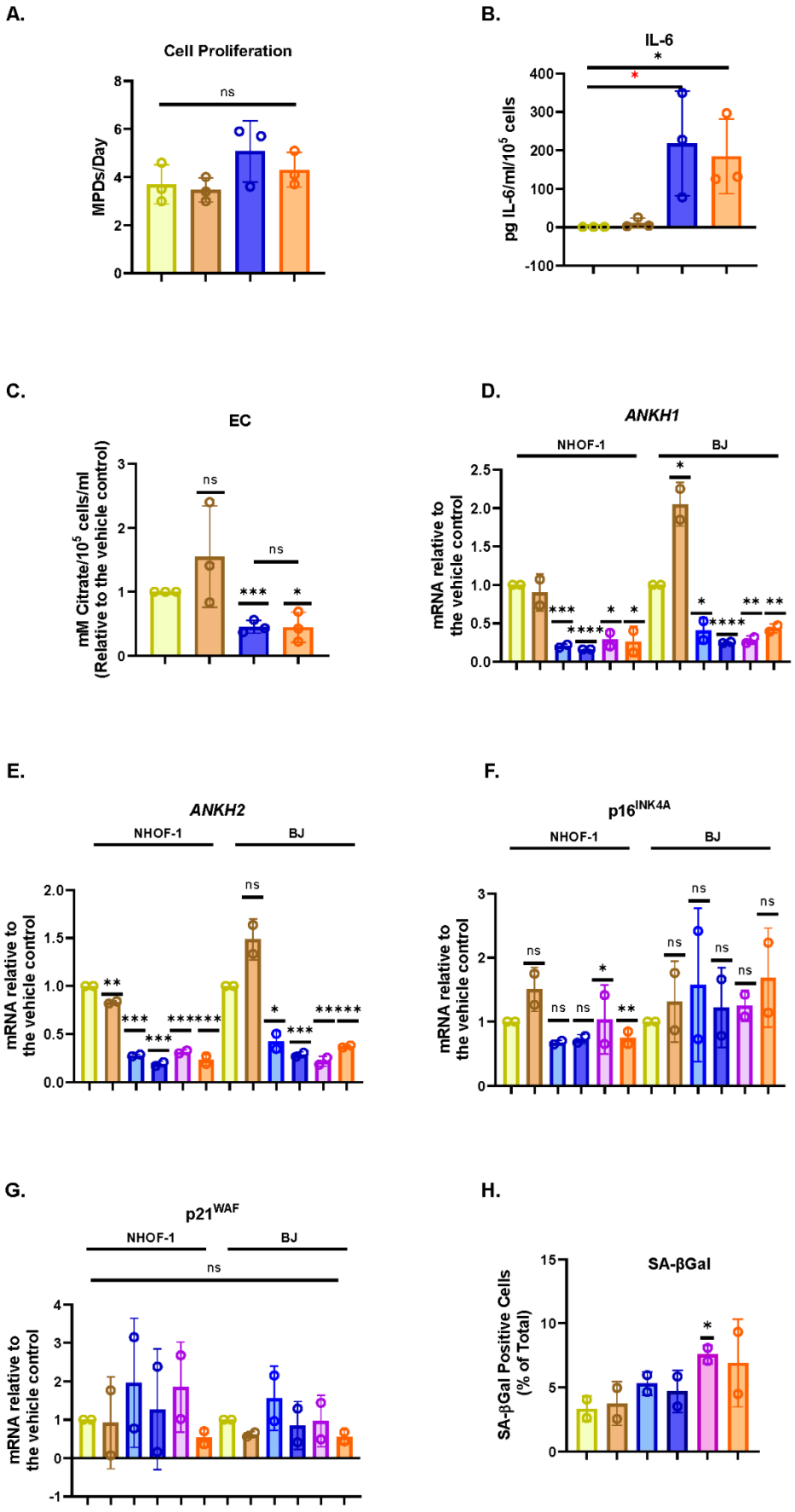
A.
Cell Proliferation
MPDs/Day
ns
B.
IL-6
pg IL-6/ml/10^5 cells
C.
EC
mM Citrate/10^5 cells/ml
(Relative to the vehicle control)
D.
ANKH1
NHOF-1
BJ
mRNA relative to
the vehicle control
E.
ANKH2
F.
p16INK4A
G.
p21WAF
H.
SA-βGal
SA-βGal Positive Cells
(% of Total)

Figure 5. The effect of IL-1α on EC, *ANKH* expression and secreted IL-6 in proliferating human fibroblasts.

The figure shows the effects of an 8-day treatment with the indicated doses of IL-1α and HC on proliferating NHOF-1 and BJ cells.

A. Shows the rate of proliferation of BJ cells in MPDs per day.

B. Shows the absolute levels of IL-6 in pg/ml per 10^5 cells in BJ cells.

C. Shows the absolute EC levels in mM citrate per 10^5 cells per ml in BJ cells.

D. The effect the indicated doses of IL-1α and 300 nM HC and on the expression of *ANKH* mRNA in BJ and NHOF-1 cells using primer set 1.

E. As in C. but the results of primer set 2 in the same experiments.

F. As in C. but the expression of the senescence marker $p16^{INK4A}$in the same experiments.

G. As in C. but the expression of the senescence marker $p21^{WAF1}$ in the same experiments.

H. The expression of senescence marker SA-βGal in the same BJ cell experiments.

A.- C. Yellow bars control; dark blue bars 1ng/ml IL-1α; brown bars 300nm HC; orange bars = 1 ng/ml IL-1α and 300nm HC.

D.-H. Yellow bars control; light blue bars 0.5 ng/ml IL-1α; dark blue bars 1ng/ml IL-1α; purple bars 2.5 ng/ml IL-1α; brown bars 300nm HC; orange bars = 2.5 ng/ml IL-1α and 300nm HC * = $P< 0.05$; ** = $P < 0.01$; *** = $P < 0.001$; ns = not significant. The results are averages +/- standard deviation. A. and B. N = 3. C-G. N=2.

The experiments in A.- C. and D.- H. were performed at different times but using identical cell culture protocols and reagents.

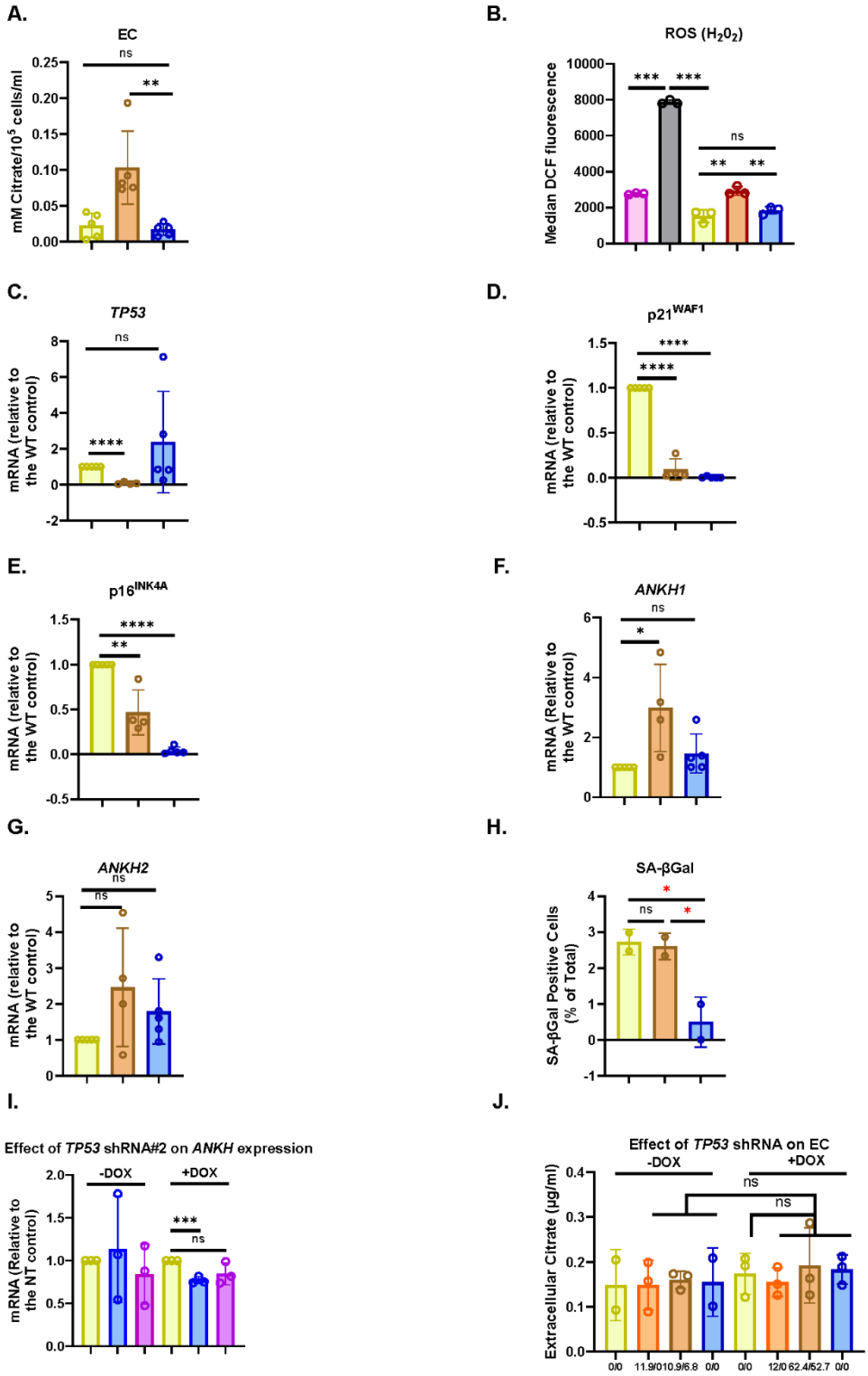
A.
EC
mM Citrate/10^5 cells/ml
ns
**
B.
ROS (H2O2)
Median DCF fluorescence
***
***
ns
**
**
C.
TP53
mRNA (relative to the WT control)
ns
****
D.
p21WAF1
mRNA (relative to the WT control)
****
****
E.
p16INK4A
mRNA (relative to the WT control)
****
**
F.
ANKH1
mRNA (Relative to the WT control)
ns
*
G.
ANKH2
mRNA (relative to the WT control)
ns
ns
H.
SA-βGal
SA-βGal Positive Cells (% of Total)
*
ns
*
I.
Effect of TP53 shRNA#2 on ANKH expression
mRNA (Relative to the NT control)
-DOX
+DOX
***
ns
J.
Effect of TP53 shRNA on EC
Extracellular Citrate (µg/ml)
-DOX
+DOX
ns
ns
0/0
11.9/0
10.9/6.8
0/0
0/0
12/0
62.4/52.7
0/0

Figure 6 The effect of the senescence effectors on EC and *ANKH* expression in human fibroblasts.

A. EC levels in wild type Loxo26 fibroblasts and their corresponding p53-/- and $p21^{WAF}$-/- null lines. N = 5.

B. ROS (mainly H_2O_2) levels as assessed by DCF fluorescence and measured on the FACS in the same cell lines as in A. (N = 3).

C. TP53 transcript abundance of the cells in A. (N = 4).

D. $p21^{WAF1}$ transcript abundance of the cells in A. N =4).

E. $p16^{INK4A}$ transcript abundance of the cells in A. N =4).

F. *ANKH1* abundance of the cells in A as assessed by the primer set 1. N =4).

G. *ANKH1* abundance of the cells in A as assessed by the primer set 2. N =4).

H. The expression of senescence marker SA-βGal in the same experiments as in A. (N =2).

A.-H. Yellow bars wild type Loxo26; orange bars p53-/- Loxo26; blue bars p21-/- Loxo26.

B. Pink bars = BJ cells; grey bars = Leiden $p16^{INK4A-}$/- cells / $p14^{ARF}$+/- cells.

I. The level of *ANKH* mRNA knockdown achieved by the *TP53* shRNAs relative to the Non-targeting (NT) control following doxycyclin (DOX) induction (*ANKH1*, blue bars), (*ANKH2*, purple bars) or control (yellow bars) in growing NHOF-1 cells. N =3.

J. The EC level in growing NHOF-1 cells relative to the non-targeting (NT) control (yellow bars), *TP53* shRNA #1 (orange bars), shRNA #2 (brown bars) and shRNA #3 (blue bars) following doxycyclin (DOX) induction (+DOX) or control (-DOX). N =3. Numbers under the bars indicate the % of *TP53*/$p21^{WAF}$ knockdown, respectively.

* = P< 0.05; ** = P < 0.01; *** = P < 0.001; * trend for significance; ns = not significant. The results are averages +/- standard deviation.

The experiments in A., B, C.- H and I.-J. were performed at separate times but using identical cell culture protocols and reagents.

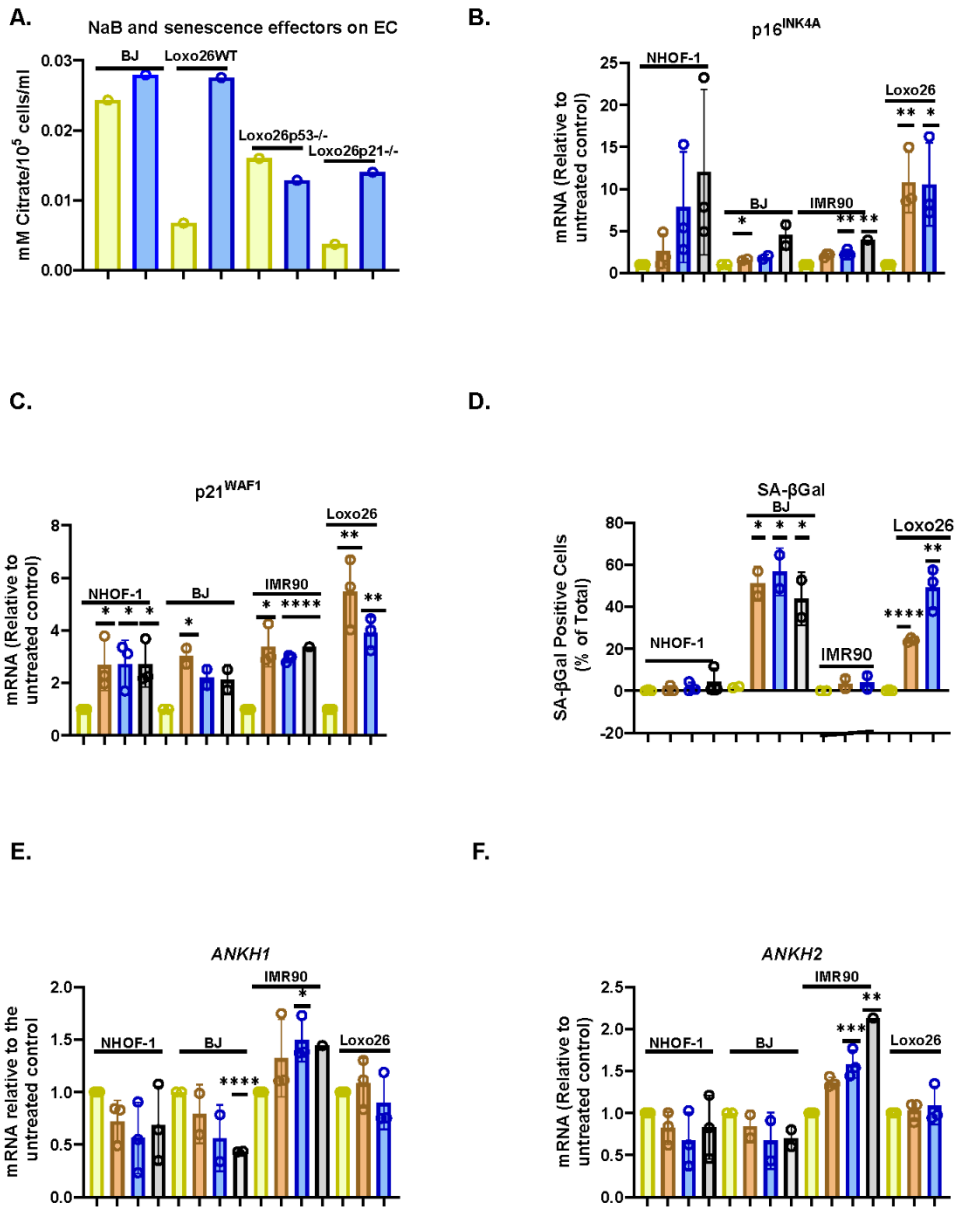
A.
NaB and senescence effectors on EC
mM Citrate/10^5 cells/ml
BJ
Loxo26WT
Loxo26p53-/-
Loxo26p21-/-
B.
p16^INK4A
mRNA (Relative to untreated control)
NHOF-1
BJ
IMR90
Loxo26
C.
p21^WAF1
mRNA (Relative to untreated control)
NHOF-1
BJ
IMR90
Loxo26
D.
SA-βGal
SA-βGal Positive Cells (% of Total)
NHOF-1
BJ
IMR90
Loxo26
E.
ANKH1
mRNA relative to the untreated control
NHOF-1
BJ
IMR90
Loxo26
F.
ANKH2
mRNA (Relative to untreated control)
NHOF-1
BJ
IMR90
Loxo26

Figure 7 The effect of sodium butyrate (NaB) on cellular senescence, EC and the expression of *ANKH* in human fibroblasts

A. A single experiment showing the effect of 0.5mM NaB on EC in BJ and Loxo26 human fibroblasts and the induction of EC only in Loxo26.

B. The effect of NaB at doses of 1-4mM for 17 days on NHOF-1, BJ, IMR90 and Loxo26 on the senescence marker $p16^{INK4A}$in the same experiments.

C. As in B. but the expression of the senescence marker $p21^{WAF1}$ in the same experiments.

D. As in B. but the expression of senescence marker SA-βGal in the same experiments

E. As in B. but the expression of *ANKH* mRNA using primer set 1.

F. As in B. but the results of primer set 2 in the same experiments.

A. Yellow bars = control light blue bars = 0.5mM NaB

B. – F. Yellow bars = control; brown bars = 1 mM; blue bars = 2 mM; grey bars = 4 mM NaB.

A. Yellow bars = control light blue bars = 0.5mM NaB * = P< 0.05; ** = P < 0.01; *** = P < 0.001; ns = not significant. The results are averages +/- standard deviation. N = 3.

The experiments in A. and B-F. were performed at separate times but using identical protocols and reagents.

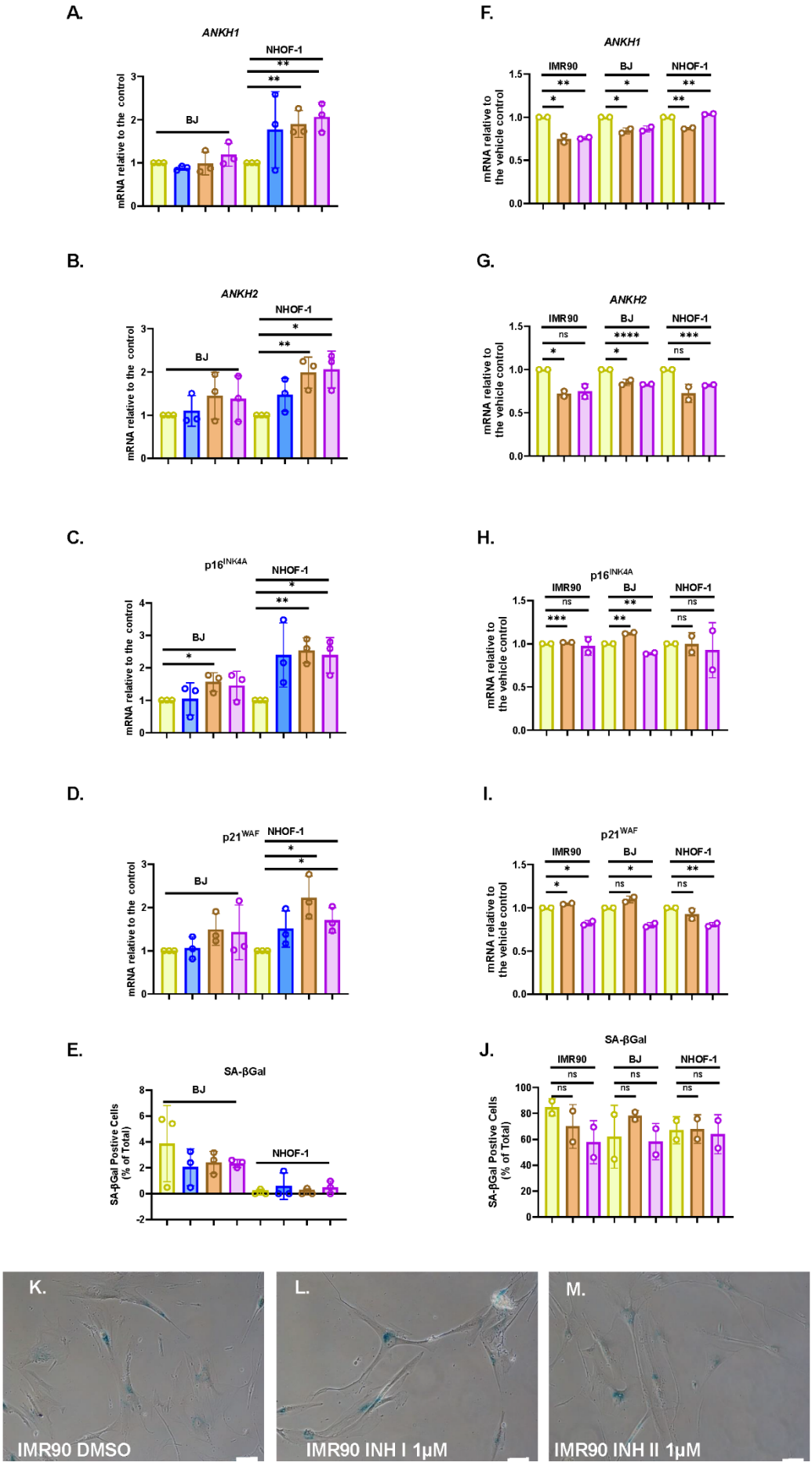
A.
ANKH1
mRNA relative to the control
BJ
NHOF-1
B.
ANKH2
mRNA relative to the control
BJ
NHOF-1
C.
p16INK4A
mRNA relative to the control
BJ
NHOF-1
D.
p21WAF
mRNA relative to the control
BJ
NHOF-1
E.
SA-βGal
SA-βGal Postive Cells (% of Total)
BJ
NHOF-1
F.
ANKH1
mRNA relative to the vehicle control
IMR90
BJ
NHOF-1
G.
ANKH2
mRNA relative to the vehicle control
IMR90
BJ
NHOF-1
H.
p16INK4A
mRNA relative to the vehicle control
IMR90
BJ
NHOF-1
I.
p21WAF
mRNA relative to the vehicle control
IMR90
BJ
NHOF-1
J.
SA-βGal
SA-βGal Postive Cells (% of Total)
IMR90
BJ
NHOF-1
K.
IMR90 DMSO
L.
IMR90 INH I 1μM
M.
IMR90 INH II 1μM

Figure 8. The effect of TGFβ on cellular senescence and the expression of *ANKH* in human fibroblasts

A.- E. The effect of TGFβ at doses of 1-10ng/ml for 4 days on NHOF-1 and BJ fibroblasts on the expression of ANKH and senescence markers in growing young fibroblasts.

A. The expression of *ANKH* mRNA using primer set 1.

B. As in A. but the results of primer set 2 in the same experiments.

C. As in A. but the expression of the senescence marker $p16^{INK4A}$in the same experiments.

D. As in A. but the expression of the senescence marker $p21^{WAF1}$ in the same experiments.

E. As in A. but the expression of senescence marker SA-βGal in the same experiments.

Yellow bars control; blue bars 1 ng/ml; brown bars 3 ng/ml ; purple bars 10ng/ml * = P< 0.05; ** = P < 0.01; *** = P < 0.001; ns = not significant. The results are averages +/- standard deviation. N = 3.

F. - J. The effect of TGFβ type I receptor kinase inhibitors on the expression of ANKH and senescence markers in IrrDSBsen IMR90, BJ and NHOF-1 fibroblasts.

F. The expression of *ANKH* mRNA using primer set 1.

G. As in A. but the results of primer set 2 in the same experiments.

H. As in A. but the expression of the senescence marker $p16^{INK4A}$in the same experiments.

I. As in A. but the expression of the senescence marker $p21^{WAF1}$ in the same experiments.

J. As in A. but the expression of senescence marker SA-βGal in the same experiments.

K. - M. Representative images of the SA-βGal staining of IMR90 cells in J.

Yellow bars vehicle control (0.1% DMSO); brown bars TGFβ type I receptor kinase inhibitor I at 1μM; purple bars TGFβ type I receptor kinase inhibitor II at 1μM.

* = P< 0.05; ** = P < 0.01; *** = P < 0.001; ns = not significant. The results are averages +/- standard deviation. N = 2 for each cell line.

A.

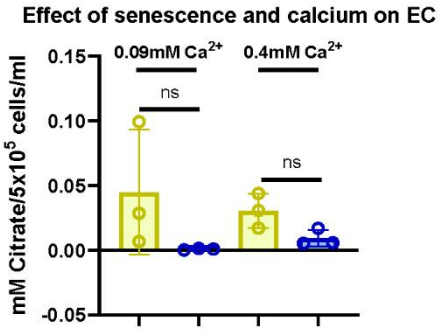
Effect of senescence and calcium on EC
0.09mM Ca2+
0.4mM Ca2+
ns
ns
mM Citrate/5x10^5 cells/ml
0.15
0.10
0.05
0.00
-0.05

B.

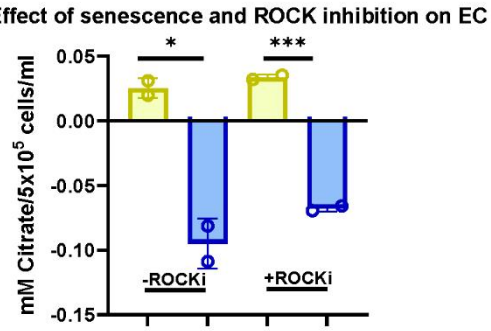
Effect of senescence and ROCK inhibition on EC
*
***
mM Citrate/5x10^5 cells/ml
0.05
0.00
-0.05
-0.10
-0.15
-ROCKi
+ROCKi

C.

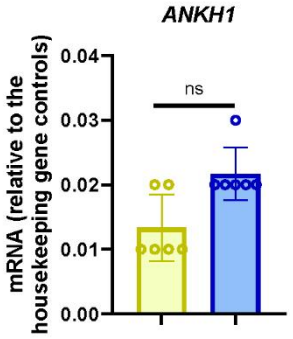
ANKH1
ns
mRNA (relative to the housekeeping gene controls)
0.04
0.03
0.02
0.01
0.00

D.

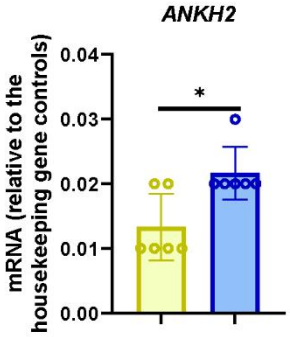
ANKH2
*
mRNA (relative to the housekeeping gene controls)
0.04
0.03
0.02
0.01
0.00

E.

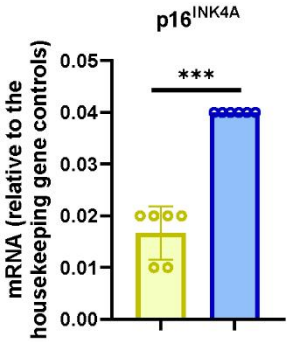
p16INK4A
***
mRNA (relative to the housekeeping gene controls)
0.05
0.04
0.03
0.02
0.01
0.00

F.

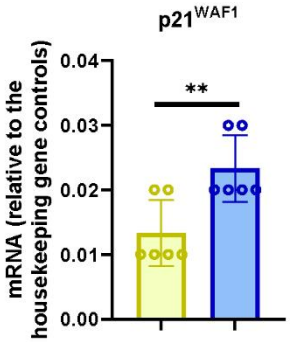
p21WAF1
**
mRNA (relative to the housekeeping gene controls)
0.04
0.03
0.02
0.01
0.00

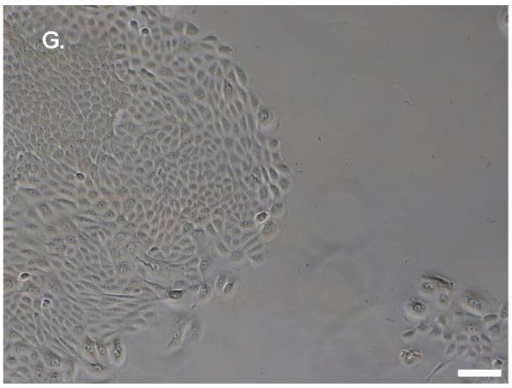
G.

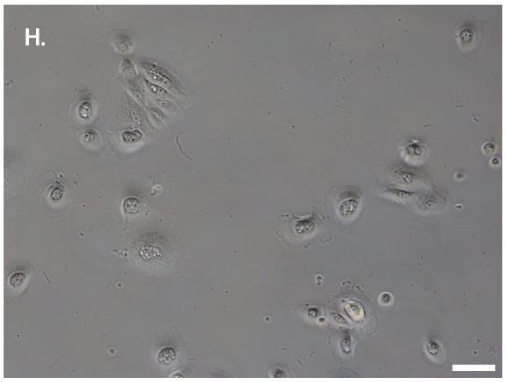
H.

Figure 9 EC and *ANKH* are not upregulated following IrrDSBsen or PEsen in hman epidermal keratinocytes

A. EC in IrrDSBsen (grey bars) and control keratinocytes (white bars) cultured in serum-free medium (N=3)

B. The same lines as in A. cultured with irradiated 3T3 feeder cells with (grey bars) and without (white bars) the ROCK inhibitor y27632. The 3T3 feeders were removed prior to the collection of the conditioned medium.

C. The expression of *ANKH* mRNA in PEsen HEK127 cells in 3 different Ca+ concentrations at 11.2 and 21.5 MPDs using primer set 1 (N = 6).

D . As in C. but the results of primer set 2 in the same experiments.

E. As in C. but the expression of the senescence marker $p16^{INK4A}$in the same experiments.

F. As in C. but the expression of the senescence marker $p21^{WAF1}$ in the same experiments.

A. Yellow bars = Control cells; blue bars = IrrDSBsen cells. 0.4mM Ca+ data stippled bars.

B. As in A. but ROCKi treated cells stippled. C-F. Yellow bars = 11.2 MPDs; blue bars = 21.5 MPDs; * = P< 0.05; ** = P < 0.01; *** = P < 0.001; * trend for significance; ns = not significant. The results are averages +/- standard deviation.

G. Image of young HEK127 (11.2 MPDs) in 0.4mM Ca+. H. Image of old HEK127 (21.5 MPDs) in 0.4mM Ca+. Bar = 100µM.

The experiments in A. and C.- G. were performed at separate times but using identical protocols and reagents. The data from C.-G. were derived from the same experiments as Figure 10 C.-F.

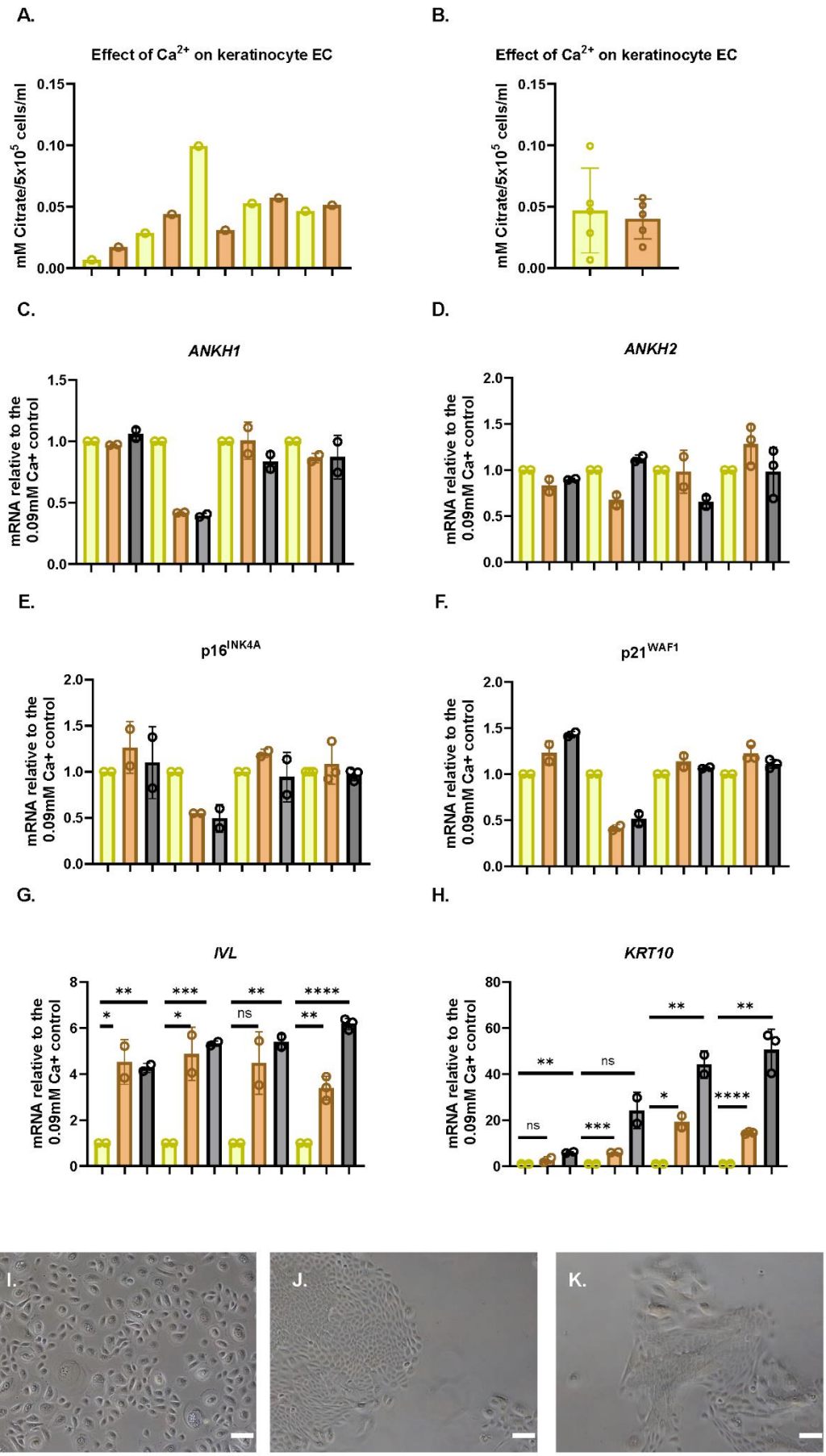
A.
Effect of Ca2+ on keratinocyte EC
mM Citrate/5x10^5 cells/ml
0.15
0.10
0.05
0.00
B.
Effect of Ca2+ on keratinocyte EC
mM Citrate/5x10^5 cells/ml
0.15
0.10
0.05
0.00
C.
ANKH1
mRNA relative to the 0.09mM Ca+ control
1.5
1.0
0.5
0.0
D.
ANKH2
mRNA relative to the 0.09mM Ca+ control
2.0
1.5
1.0
0.5
0.0
E.
p16INK4A
mRNA relative to the 0.09mM Ca+ control
2.0
1.5
1.0
0.5
0.0
F.
p21WAF1
mRNA relative to the 0.09mM Ca+ control
2.0
1.5
1.0
0.5
0.0
G.
IVL
mRNA relative to the 0.09mM Ca+ control
8
6
4
2
0
**
*
***
*
**
ns
****
**
H.
KRT10
mRNA relative to the 0.09mM Ca+ control
80
60
40
20
0
**
ns
ns
***
**
*
**
****
I.
J.
K.

Figure 10 EC and *ANKH* are not upregulated during keratinocyte differentiation.

A. The effect of 0.4mM Ca+ on EC in five different epidermal keratinocyte lines in serum-free medium.

B. The average of the results in A. +/- standard deviation (n =5); ns = not significant.

C. The expression of *ANKH* mRNA in four epidermal lines in 3 different Ca+ concentrations

D. As in C. but the results of primer set 2 in the same experiments.

E. As in C. but the expression of the senescence marker $p16^{INK4A}$in the same experiments.

F. As in C. but the expression of the senescence marker $p21^{WAF1}$ in the same experiments.

G. As in C. but the expression of the differentiation marker INV in the same experiments.

H. As in C. but the expression of the terminal differentiation marker K10 in the same experiments.

Yellow bars = 0.09mM Ca+ cells; brown bars = 0.4mM Ca+ dark grey bars = 1.0mM Ca+. * = P< 0.05; ** = P < 0.01; *** = P < 0.001; * trend for significance; ns = not significant. The results are averages +/- standard deviation (N =3).

I. Image of young HEK127 (11.2 MPDs) in 0.09mM Ca+ J. Image of the same cells as in I. in 0.4mM Ca+ (the same image as Figure 9G). K. Image of the same cells as in I. in 1.0mM Ca+.

The experiments in A.-B. and C.- H. were performed at separate times but using identical protocols and reagents. The data from C.-H. were derived from the same experiments as Figure 9 C.-G.

A.

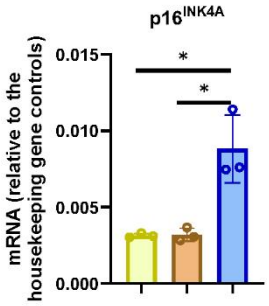
p16INK4A
mRNA (relative to the housekeeping gene controls)
0.015
0.010
0.005
0.000
*
*

B.

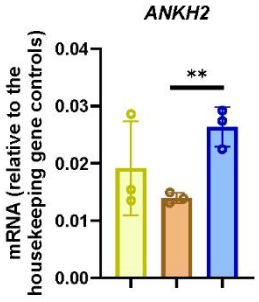
ANKH2
mRNA (relative to the housekeeping gene controls)
0.04
0.03
0.02
0.01
0.00
**

C.

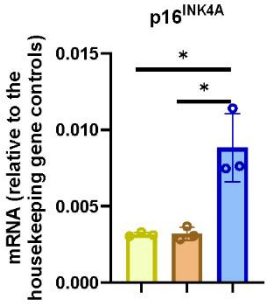
p16INK4A
mRNA (relative to the housekeeping gene controls)
0.015
0.010
0.005
0.000
*
*

D.

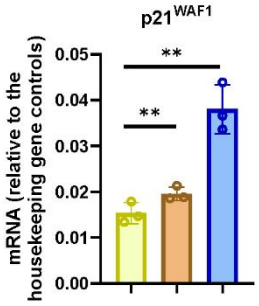
p21WAF1
mRNA (relative to the housekeeping gene controls)
0.05
0.04
0.03
0.02
0.01
0.00
**
**

E.

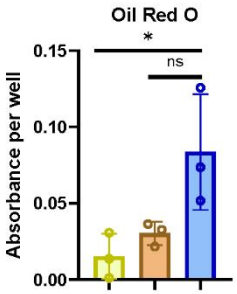
Oil Red O
Absorbance per well
0.15
0.10
0.05
0.00
*
ns

F.

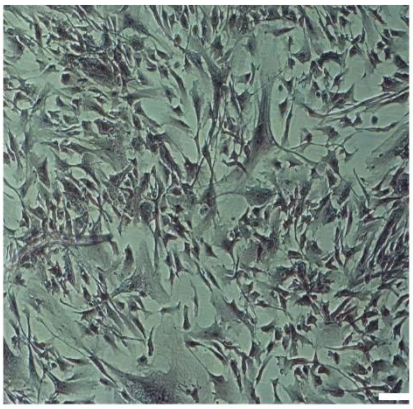

G.

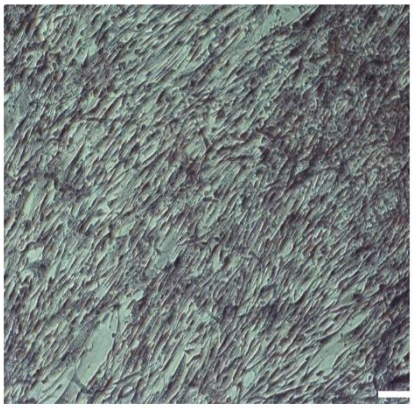

H.

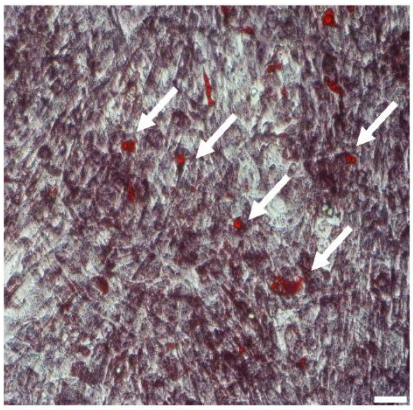

I.

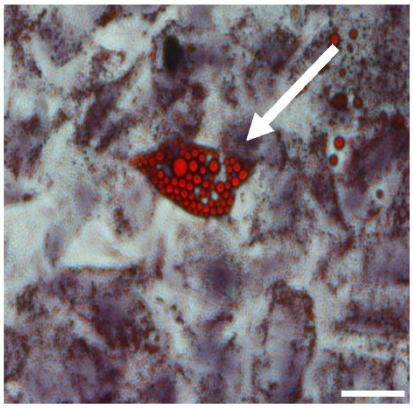

Figure 11 *ANKH* mRNA is upregulated in differentiated adipocytes following confluence-induced senescence.

A. The expression of *ANKH* mRNA using primer set 1.

B. The expression of *ANKH* mRNA using primer set 2.

C. The expression of $p16^{INK4A}$ mRNA.

D. The expression of $p21^{WAF1}$ mRNA.

E. Oil Red O staining to indicate adipocyte differentiation.

Yellow bars = young growing control; brown bars = young confluent (4 days control); blue bars = confluent (15 days) senescent differentiated adipocytes.

* = P< 0.05; ** = P < 0.01; *** = P < 0.001; * trend for significance; ns = not significant. The results are averages +/- standard deviation. N = 3.

F. Young growing control. G. Young confluent control. H. Young confluent differentiated showing cells with Oil Red-positive lipid droplets (arrows). Bar = 100µM. I. A higher power image of H. Bar = 100µM.

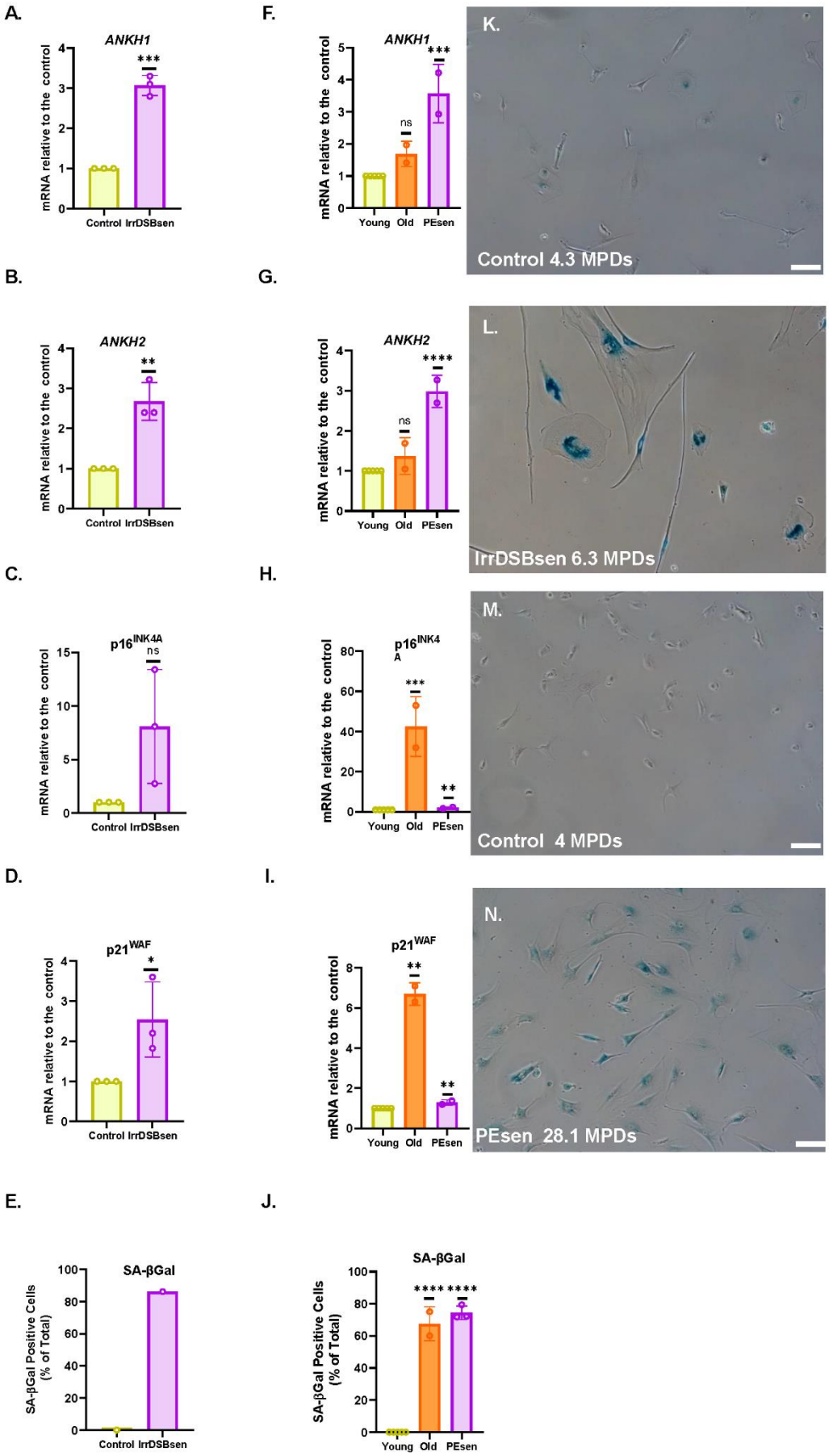
A.
ANKH1
mRNA relative to the control
***
Control
IrrDSBsen
B.
ANKH2
**
C.
p16INK4A
ns
D.
p21WAF
*
E.
SA-βGal
SA-βGal Positive Cells (% of Total)
F.
Young
Old
PEsen
G.
****
H.
I.
J.
K.
Control 4.3 MPDs
L.
IrrDSBsen 6.3 MPDs
M.
Control 4 MPDs
N.
PEsen 28.1 MPDs

Figure 12 *ANKH* mRNA is differentially regulated in IrrDSBsen and PEsen astrocytes

A.- E. IrrDSBsen; F-J. PEsen.

A. and F. The expression of *ANKH* mRNA using primer set 1.

B. and G The expression of *ANKH* mRNA using primer set 2.

C. and H. The expression of $p16^{INK4A}$ mRNA.

D. and I. The expression of $p21^{WAF1}$ mRNA.

E. and J. SA-β Gal expression (%).

Yellow bars A.-J. = Young growing control; purple bars A.-E. = IrrDSBsen; F-J PEsen astrocytes (27-28.9 MPDs). F-J. orange bars = old (22-23 MPDs) astrocytes. * = P< 0.05; ** = P < 0.01; *** = P < 0.001; **** = P < 0.0001; * trend for significance; ns = not significant. The results are averages +/- standard deviation. A- D N = 3; E is the result of a single experiment; F-J N = 2.

K. and L. Representative images of SA-βGal staining in E; K. Young growing astrocytes (4.3 MPDs), L. IrrDSBsen astrocytes (6.3 MPDs). M. and N. Representative images of SA-βGal staining in J. M. Young growing astrocytes (4.0 MPDs), N. PEsen astrocytes (28.1 MPDs): Bar = 100µm.

A.

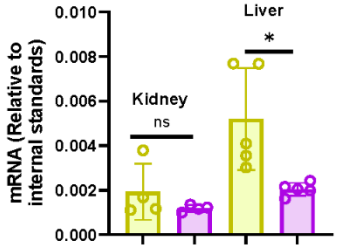
mRNA (Relative to internal standards)
0.010
0.008
0.006
0.004
0.002
0.000
Kidney
ns
Liver
*

B.

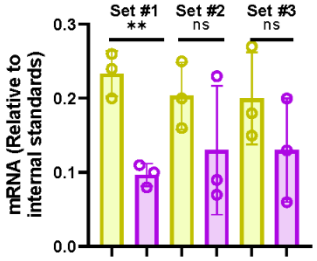
mRNA (Relative to internal standards)
0.3
0.2
0.1
0.0
Set #1
**
Set #2
ns
Set #3
ns

C.

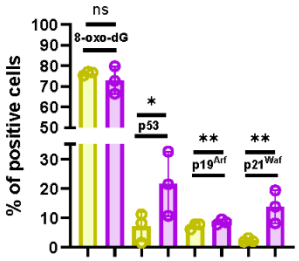
% of positive cells
100
90
80
70
60
50
30
20
10
0
ns
8-oxo-dG
*
p53
**
p19Arf
**
p21Waf

D.

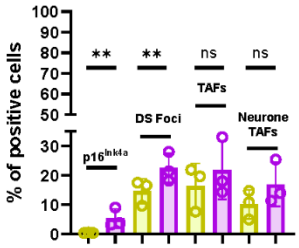
% of positive cells
100
90
80
70
60
50
30
20
10
0
**
p16Ink4a
**
DS Foci
ns
TAFs
ns
Neurone TAFs

E.

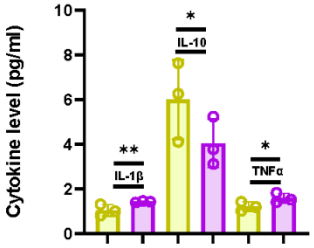
Cytokine level (pg/ml)
10
8
6
4
2
0
**
IL-1β
*
IL-10
*
TNFα

F.

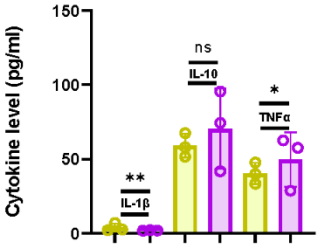
Cytokine level (pg/ml)
150
100
50
0
**
IL-1β
ns
IL-10
*
TNFα

G.

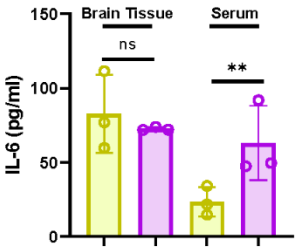
IL-6 (pg/ml)
150
100
50
0
Brain Tissue
ns
Serum
**

H.

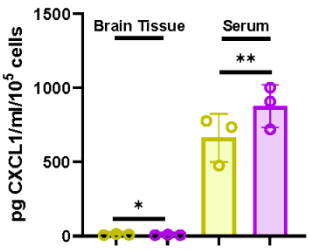
pg CXCL1/ml/10^5 cells
1500
1000
500
0
Brain Tissue
*
Serum
**

Figure 13 Age mouse tissues show increased levels of senescence markers and inflammatory cytokines in parallel with reduced levels of *ANKH* mRNA.

A. *ANKH* mRNA levels in young (4 month) and old (25 month) kidney (N = 4) and liver (N =5) tissue.

B. *ANKH* mRNA levels in young (2.5 month) and old (17 month) brain tissue (N =3).

C. Immunofluorescence staining of adult and aged C57BL/6 mice. (A) Percentage of cells expressing 8-oxo-dg, (B) Percentage of cells expressing p53, (C) Percentage of cells expressing $p21^{Waf1}$, (D) Percentage of cells expressing $p19^{Arf}$.

D. Immunofluorescence staining of adult and aged C57BL/6 mice. (A) Percentage of cells expressing $p16^{Ink4a}$, (B) Percentage of cells expressing γH2AX.53BP1 double foci (DF), (C) Percentage of cells expressing telomere-associated foci (TAF), (D) Percentage of neurons expressing TAF.

E. Different cytokine levels (pg/mL) in brain samples. Interleukin-1 beta (IL-1β), Interleukin-10 (IL-10), Tumour necrosis factor alpha (TNF-α).

F. Different cytokine levels (pg/mL) in serum samples. (Interleukin-1 beta (IL-1β), Interleukin-10 (IL-10), (C) (E) Tumour necrosis factor alpha (TNF-α).

G. IL-6 levels (pg/ml) in brain and serum samples.

H. CXCL1 levels (pg/ml) in brain and serum samples.

A. and B. Results analysed by the Student's two-tailed unpaired test. * = P< 0.05; ** = P < 0.01; *** = P < 0.001; ns = not significant. The results are averages +/- standard deviation.

C.-H. Results represent the median, minimum and maximum. Data were analysed using the Mann-Whitney U test; *p<0.05. 3 animals for Adult C57BL/6, and 3 animals for Aged C57BL/6.

A. Yellow bars = young (4-month-old mice); purple bars = old (25-month-old mice).

B.– H. Yellow bars = young (2.5-month-old mice); purple bars = old (17-month-old mice).

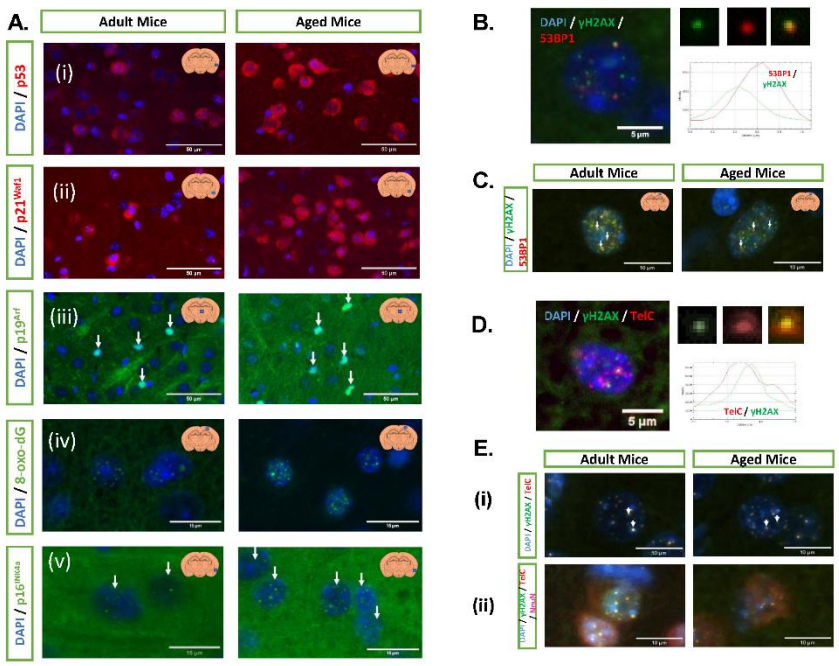

Figure 14 Immunofluorescence staining of multiple cellular senescence markers.

A. Representative images of (i) p53 signal in the cerebral cortex, (ii) $p21^{Waf1}$ signal in the cerebral cortex, (iii) $p19^{Arf}$ signal in the thalamus, (iv) 8-oxo-dG signal in the cerebral cortex, (v) $p16^{INK4a}$ signal in the cerebral cortex. All images were taken at 20X magnification. Bar = 50µm.

B. Example of γH2AX and 53BP1 signals in a nucleus, the arrow demonstrates a DF, and the histogram displays their overlap.

C. Representative images of both groups.

D. Examples of TAF, γH2AX and TelC signals in a nucleus, the arrow demonstrates a DF, and the histogram displays their overlap.

E. Representative images of TAF in a (i) nucleus, (ii) neuron. Images from B. to E. were taken at 60X magnification. Bar = as indicated on the image.